Abstract

To find exoplanets, it is important to have accurate measurements for potential host stars to make it easier to tell when something changes that might indicate the presence of an exoplanet. A-type stars, which have up to about twice the mass of our Sun, rotate very fast, making it hard to see if an exoplanet's gravity is tugging on them. However, when these stars have aged and cooled into subgiants, they rotate slower, making it easier to spot planets around them. This project uses near-infrared data from Georgia State University's Center for High Angular Resolution Astronomy (CHARA) on Mount Wilson, CA, to accurately measure the radii of five retired A stars. Models make it possible to predict the stars' luminosity, temperature, age, and mass from the radii measurements. The measurements of these five properties are then compared to the properties estimated by existing literature, which generally uses broad-band photometric data and derives the radius using a chart rather than measuring it directly. Hypothetically, there will be a systematic offset in the measured values as compared to the literature values. This comparison will help to refine the models and lead to more accurate measurements of retired A star radii — and lead to more exoplanet discoveries.

What Are the True Sizes of Retired A Stars?

Authored by Lauren Leese

Thesis Advisor:

Darby Dyar, Mount Holyoke College

Submitted to the Department of Astronomy at Mount Holyoke College

with the purpose of honors consideration

ACKNOWLEDGEMENTS

First and foremost, a huge thank-you to my Louisiana State University Physics and Astronomy Research Experience for Undergraduates mentor, Dr. Tabetha Boyajian. I'm so grateful that she trusted me with this project and helped me see it through. This thesis would not exist without her help, guidance, and patience. I am also grateful for the pottery nights and the lovely mugs.

Thank you also to Dr. Tyler Ellis, whose v2fit code was indispensable for this project. I am extremely appreciative of the time he took to help me calibrate the data using his program. I am also very thankful for that one time he bought me a chai latte on my first week of researching at LSU when I was shy and didn't know anyone.

Thank you to Darby Dyar, my Astronomy faculty advisor and my advisor for this thesis, whose feedback was invaluable to me. I will forever be grateful to her for seeing something in me as a scared little first-year student and encouraging me to pursue more astronomy classes. Her instruction has pushed me to new heights as a writer and as a student of science.

Thank you to Jason Young, my astrophysics professor for my first three years at Mount Holyoke, whose patience, empathy, and excellent teaching skills are responsible for supporting and uplifting me as I completed a degree I never thought I was smart enough to attempt.

I acknowledge support from the REU Site in Physics and Astronomy (NSF Grant No. 2150445) at Louisiana State University. This work is based upon observations obtained with the Georgia State University Center for High Angular Resolution Astronomy Array at Mount Wilson Observatory. The CHARA Array is supported by the National Science Foundation under Grant

No. AST-1636624 and AST-2034336. Institutional support has been provided from the GSU College of Arts and Sciences and the GSU Office of the Vice President for Research and Economic Development.

The Mount Wilson Observatory sits on the stolen land of the Garielino, Tongva and Kizh Nations, who still reside in the Los Angeles area. The modern practice of astronomy is built on the exploitation and genocide of native peoples, and will continue thrive off of injustice for as long as telescopes continue to be operated on stolen (and often sacred) land. Thus, the Land Back movement is essential not just for repairing some of the damage done by the U.S. colonial project, but for ensuring that scientific progress does not come at the cost of human rights.

Furthermore, I performed the bulk of the data processing for this thesis at Louisiana State University, which sits on land native to many Indigenous peoples including the Caddo Adai Indians of Louisiana, Biloxi Chitimacha Confederation, Chitimacha Tribe of Louisiana, Choctaw Nation, Coushatta Tribe, Four Winds Cherokee Tribe, Muscogee (Creek), Point au Chien Tribe, Tunica Biloxi Tribe, and United Houma Nation. I wrote this thesis at Mount Holyoke College, which is located on the ancestral land of the Nonotuck people.

Table of Contents

Table of Figures

Table of Tables

1 INTRODUCTION

For as long as humanity has looked to the stars, we have asked the question, “Are we alone?” In terms of the search for life, the jury is still out; but in terms of other planets, we certainly are not. Over 5,000 exoplanets — planets that orbit stars other than our Sun — have been detected by astronomers, and millions more are surely waiting to be discovered. Perhaps Earth’s twin is even somewhere out there.

Finding more exoplanets, however, requires an understanding of the stars they orbit. It is no easy task to identify relatively tiny objects around relatively enormous objects at a distance of many parsecs from Earth. Astronomers need exceedingly accurate measurements for the physical properties of possible host stars to find tiny changes that may indicate the presence of an exoplanet. Host star properties can also reveal information about their planetary companions such as mass, size, and atmosphere composition.

It is impractical to painstakingly measure the properties of every single star in the sky. Some quantities cannot be measured from Earth. Models derived from known astrophysical relationships allow astronomers to directly measure only one physical characteristic of a star — for example, its color — and derive other measurements based on that observed attribute. As a result, there are far more data on far more stars than could be obtained only using direct observations. These data are invaluable for finding exoplanets.

There is only one issue: data derived from models are only as good as the models.

Unlike with some other scientific disciplines, astronomical models are difficult to test experimentally. For example, there is insufficient technology to fly out to a distant star and put it on a cosmic set of scales to directly measure its mass. Most astronomical observations in the optical and near-infrared spectra involve taking images of stars and measuring their light — the

techniques of photometry and spectroscopy both fall into this category. These results are then used to determine other properties about the star. To check whether the current models are doing a good job of estimating star properties, then, something other than the star's light or spectrum must be measured to see if the models deliver satisfactory results with this new input.

Enter the technique of interferometry. A full discussion of this technique is presented in Chapter 2, but interferometry involves using multiple beams of light to obtain interference fringes which can then be measured to infer the size of something. Many disciplines of physics make use of interferometry, but in astronomy, it can be used to directly measure the angular diameter of a nearby star on the sky.

Properties of various groups of stars can have an effect on exoplanet formation — most notably, planet occurrence may be related to the host star's mass (Mulders et al., 2015). It is common for exoplanet studies to look at specific masses of stars. In the past, the focus on finding Earth-like planets led to a focus on Sun-like stars for exoplanet studies, but studies of other types of stars are on the rise. The stars of interest for this thesis are a group of giant stars known as retired A stars. They represent a category of star up to twice as massive as our Sun which rotate rapidly during their main lifetime, making it difficult to locate exoplanets around them. When these stars have aged and cooled into a type of later-stage star known as a subgiant, their rotation slows. Most research on exoplanets orbiting A-type stars must be performed on these retired A stars.

This thesis describes the use of interferometry data from Georgia State University's near-infrared CHARA array to directly measure the angular diameters of five retired A stars with properties that have been well studied in the literature. Quantities such as mass, radius, and luminosity are derived from these diameters. These quantities are then compared to other studies

of these stars that have been performed using photometric methods that directly measure quantities like color instead. This thesis asks the question, is there a difference between values derived from directly-measured angular diameters and values derived from directly-measured light spectra? If so, is there a systematic difference that might indicate that existing models have missed something big? Ultimately, this work explores the accuracy of current observational techniques, paving the way for more precise measurements of retired A star properties and further exoplanet discoveries.

Chapter 2 of this thesis covers the process of interferometry and how it differs from photometry and spectroscopy, as well as the background about why retired A stars are of such interest when it comes to exoplanets. Chapter 3 discusses the details of the CHARA array and the calibration, fitting, and modeling techniques used to process the data. Results, including the measurements for the five target stars' angular diameters and their consequent estimated radii, temperatures, luminosities, masses, and ages, are discussed in Chapter 4. In Chapter 5, these results are compared to the measurements found in other studies that observed the stars using photometry rather than interferometry, and the differences are quantified using statistical techniques. Finally, Chapter 6 reflects on the ultimate result of the project, the limitations of this research, and questions that have yet to be answered about the findings.

1.1 References

Mulders, Gijs D., et al. "A stellar-mass-dependent drop in planet occurrence rates." The Astrophysical Journal, Vol. 798, No. 2 (2015)

2 BACKGROUND

This chapter covers the methods for finding stellar radii with photometry, spectroscopy and interferometry, the latter of which is the most direct measurement of stellar radii. Further discussion includes the properties of retired A stars, the Doppler spectroscopy method of exoplanet detection, and why there are questions about the prevalence of exoplanets around retired A stars.

2.1 Determining Stellar Radius from Photometry and Spectroscopy

Before discussing interferometry — the observational method used in this thesis — it is first necessary to briefly outline photometric and spectroscopic methods for finding the radius of a star. Neither of these methods involves directly measuring the radius. Instead, other parameters are directly measured and related to the radius through models and equations.

2.1.1 Finding Stellar Radii with Photometry

Photometry is the process of collecting light from a star and measuring the flux to find out how bright it appears from Earth. A photographic instrument, such as a charge-coupled device (CCD), is attached to a telescope and measures how many photons hit each pixel. This information can be transferred into electronic form for data reduction and analysis.

While photometry does not separate light into its spectra by wavelength, different filters can be used to capture specific wavelengths. The fluxes in these filters can be subtracted from each other to get a measurement of color for a star. In turn, color can be used to obtain a temperature estimate.

Figure 2-1 shows an example of a temperature-color relationship from Mucciarielli et al. (2021), a paper that uses photometry data to obtain stellar temperatures. Different colors on the graph indicate stars of different metallicities, or Fe/H, a quantity that measures the percentage of elements other than hydrogen or helium in a star. The upper pane shows stars that are still powered by core hydrogen fusion, or "dwarfs," and the lower pane shows stars that have ceased hydrogen fusion in their cores, known as "giants." The y axis shows the effective temperature of the stars in Kelvin, and the x axis shows the color of the stars as determined by the difference between two filters.

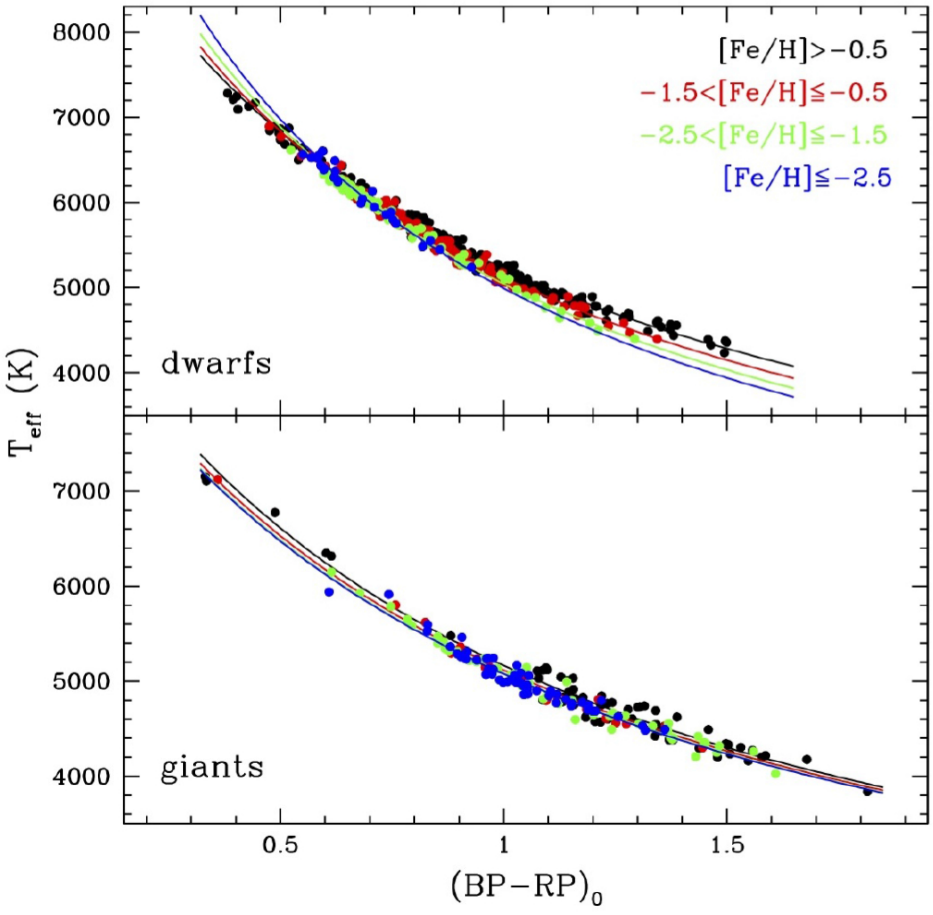

Figure 2-1: Example of an effective temperature and color relationship. Taken from Mucciarelli et al. (2021).

Bolometric luminosity refers to the total power output of a star in all wavelengths, and is often only obtainable with a distance measurement and some kind of bolometric correction. If the bolometric luminosity is known, an estimate of the stellar radius can be found by a rearrangement of the Stefan-Boltzmann Law:

$$\frac{R}{R_\odot} = (\frac{T_\odot}{T})^2 \cdot (\frac{L}{L_\odot})^{1/2}$$

In this equation, R refers to the radius of the target star, $R_\odot$ refers to the radius of the Sun, T refers to the target star temperature, $T_\odot$ refers to the radius of the Sun, L refers to the bolometric luminosity of the target star, and $L_\odot$ refers to the bolometric luminosity of the Sun. The variables relating to the Sun are well measured and may be considered knowns.

Note that the Stefan-Boltzmann Law assumes the star is a perfect black body (an object that gives off light entirely due to its heat), which is not true in practice. Accurate radius measurements require the use of stellar models to account for more sophisticated parameters.

2.1.2 Finding Stellar Radii With Spectroscopy

Like photometry, spectroscopy is concerned with collecting light. Unlike photometry, spectroscopy involves separating light into different wavelengths using a tool such as a prism. This can provide information about the chemical composition, gas pressure, magnetic field strength, and temperature of stars (Chromey, 362).

Spectral lines are not perfectly straight — they typically consist of a core with wings on either side. Figure 2-2 illustrates some examples of spectral lines for stars of different types. The x axis shows the wavelength, λ, and the y axis shows the logarithm of the flux, which indicates the intensity of each part of the spectrum.

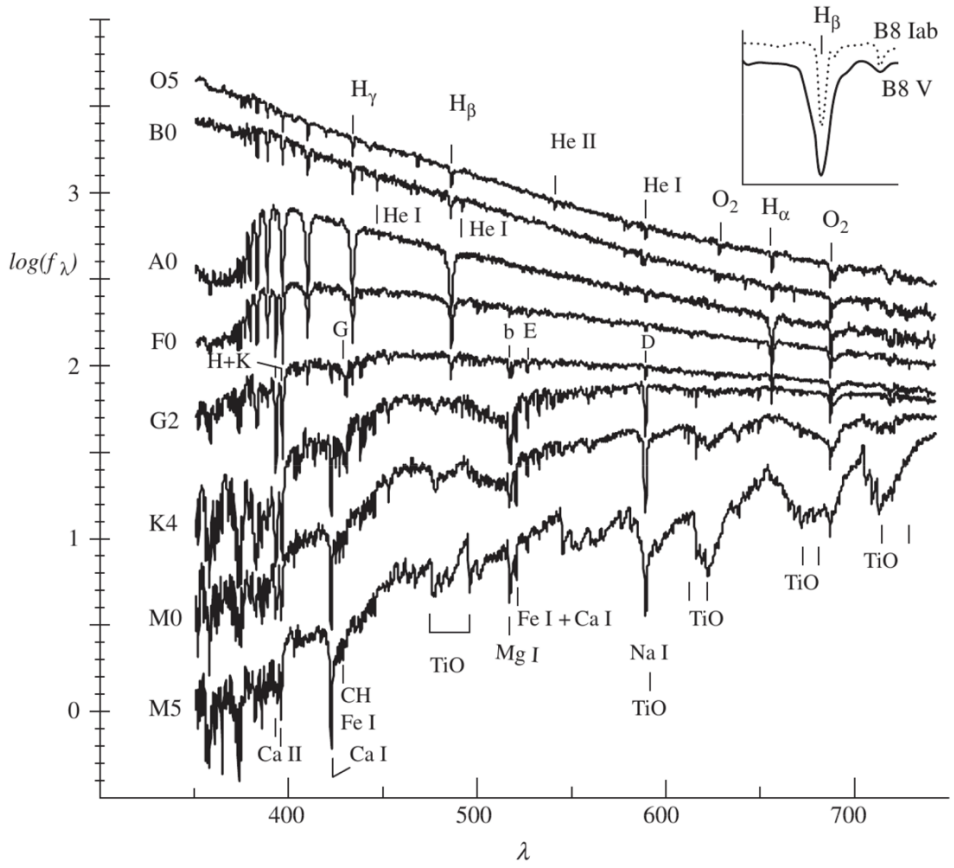

Figure 2-2: Examples of stellar spectra at 350-750 nm. Taken from Chromey's "To Measure the Sky" (Figure 11.25, made with data from Jacoby et al. (1984)).

A few different factors can cause the wings of spectral lines to broaden, but the strongest cause is pressure broadening (Chromey, 402). Studying the effect of pressure broadening on the wings allows estimation of gravitational acceleration in the photosphere of a star (Chromey, 402). If the mass of the star is also known, the stellar radius can be estimated using the equation:

$$a = \frac{GM}{R^2}$$

Here, a refers to gravitational acceleration, G refers to the gravitational constant, M refers to the mass of the star, and R refers to the radius of the star.

This stellar radius is subject to uncertainty from the gravitational acceleration estimate and whatever method was used to calculate stellar mass. A more accurate stellar radius can be obtained from spectral data through the use of modelling. These models may involve the use of astrophysical equations, but they also often involve the use of theoretical spectra for stars with known physical parameters. The target star spectrum can be compared with a variety of synthetic spectra see how well they match. If a synthetic spectrum looks similar to the target star spectrum, it may mean the target star has similar parameters to the theoretical star that produced the synthetic spectrum.

Often, parameters such as the effective temperature, surface gravity, and metallicity of a star are first determined from the spectra, then a further model is used to obtain the radius.

2.2 Determining Stellar Radius with Interferometry

Instead of directly measuring light, interferometers measure the visibility of a star by recording the interference fringes caused by starlight hitting one detector slightly before the other. This gives a measurement for the angular diameter of the star on the sky, often given in milli-arcseconds (mas). The sky can be thought of as a curved dome, which is why the diameter of a star is given as an angle rather than a distance measurement. The angular diameter can be used to find the radius through simple trigonometry using the star's distance, making it a more direct measurement of radius than photometric or spectroscopic methods.

2.2.1 Visibility

An interferometer provides a measure of a star's visibility, which is measured on a scale between 0 and 1. A visibility of 0 means the star is completely resolved and 1 means the star is

completely unresolved. An unresolved star (with a visibility closer to 1) looks like a point source, while a resolved star (with a visibility closer to zero) looks like a circle on the sky for which angular diameter can be measured. In interferometry, the ideal target is a perfectly resolved star.

2.2.2 How Interferometers Collect Data

Interferometry arrays involve two or more telescopes collecting light from the same star. The observation's baseline is the distance between the telescopes *from the perspective of the star*. That is, the baseline must account for foreshortening.

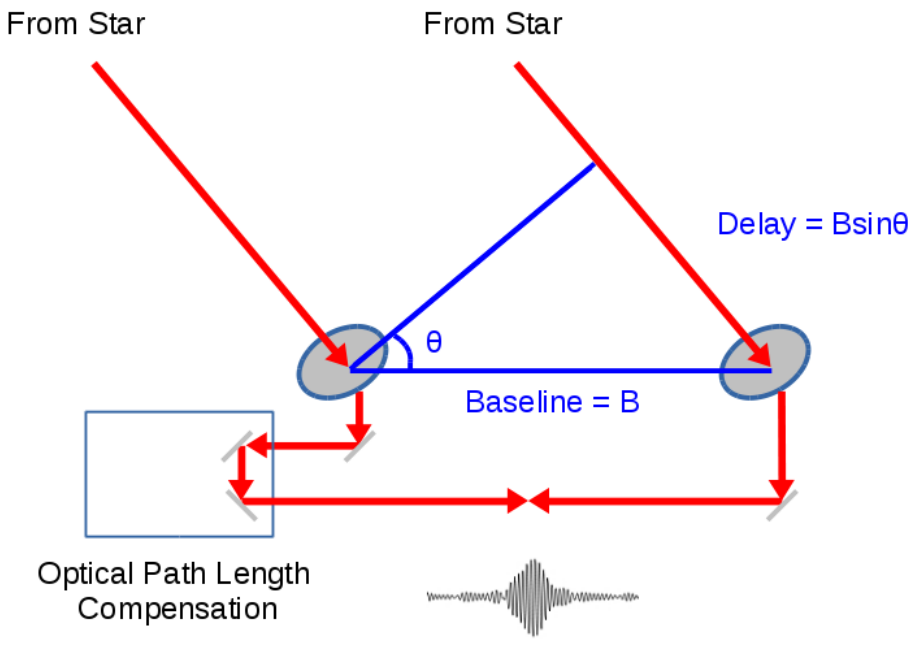

Figure 2-3: A diagram of how light is collected by CHARA. Taken from "Basics of Interferometry.

Raw interference fringes create a pattern that is encoded into data. The amplitude and contrast, or visibility, of the fringes can be used to determine information about the star being observed (“Basics of Interferometry”).

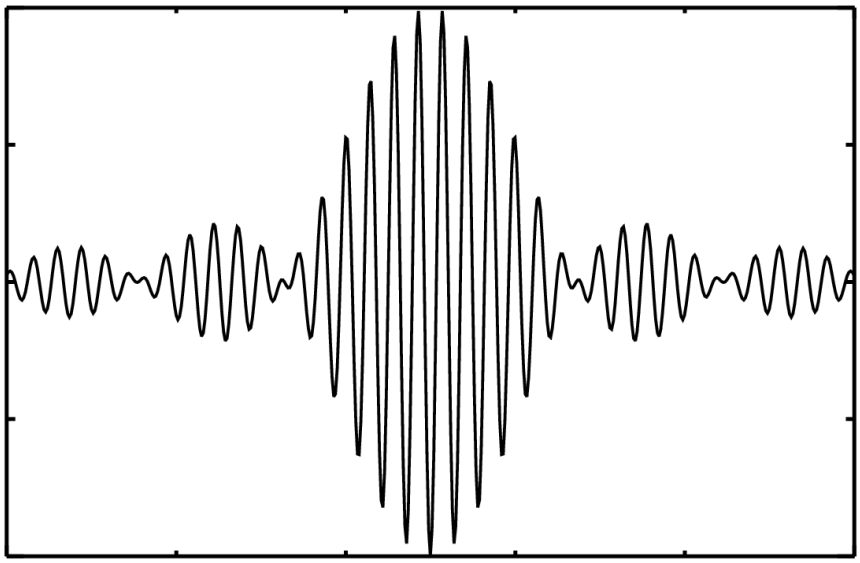

Figure 2-4: An example of interference fringes. Taken from "Basics of Interferometry."

2.2.3 Making Sense of Interference Fringes

A completely unresolved star with a visibility of 1 will have very high contrast fringes, while a resolved star will have lower-contrast fringes (“Basics of Interferometry”). Fringes are smaller with lower amplitude for bigger stars, and vice versa for smaller stars (“Basics of Interferometry”).

For visibility curves such as the example in Figure 2-5, the section of the curve before the function hits the lowest baseline with zero visibility can be measured to find the size of the star (“Basics of Interferometry”). The subsequent humps on the graph are caused by other features of the star: “limb-darkening, gravity darkening, starspots, and convection cells” (“Basics of

Interferometry"). The first lobe on the graph is the most important for finding the angular diameter.

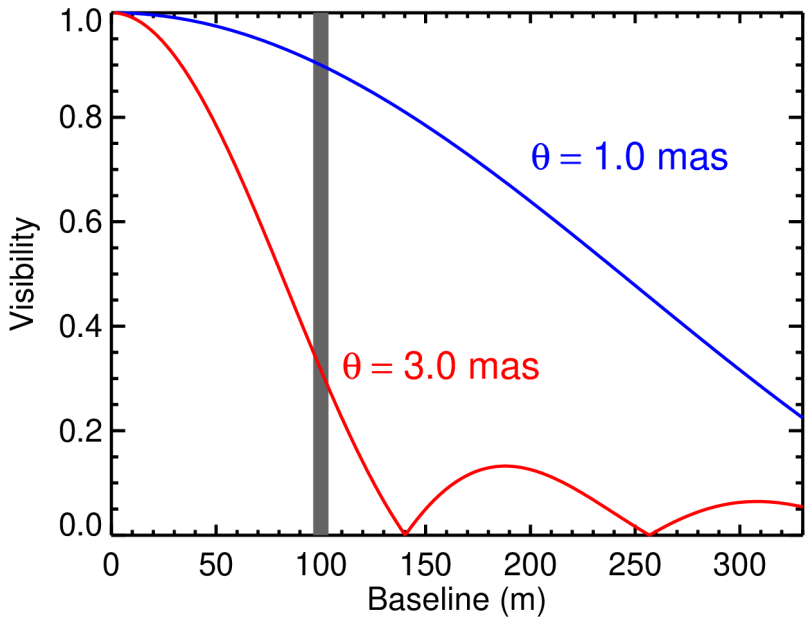

Figure 2-5: Visibility curves for a star with an angular diameter of 3.0 mas and a star with an angular diameter of 1.0 mas. For the star with an angular diameter of 3.0 mas, the section of the curve that shows the size of the star comes between a baseline of 0 and a baseline of 140. Taken from "Basics of Interferometry."

2.2.4 Limb-Darkened Disks versus Uniform Disks

The interferometer observes the star as though it is a solid circle on the sky. In reality, the star's envelope extends beyond the uniform disk, or UDD, recorded in the given wavelength. A limb-darkened disk, or LDD, refers to the true angular diameter of the star after taking the envelope into account.

The extent of a stellar envelope depends on factors such as the star's temperature, metallicity, and surface gravity. Transforming a UDD to an LDD requires the use of model-

based calculations, but this is the only part of the angular diameter-measuring process that does not rely on direct observation.

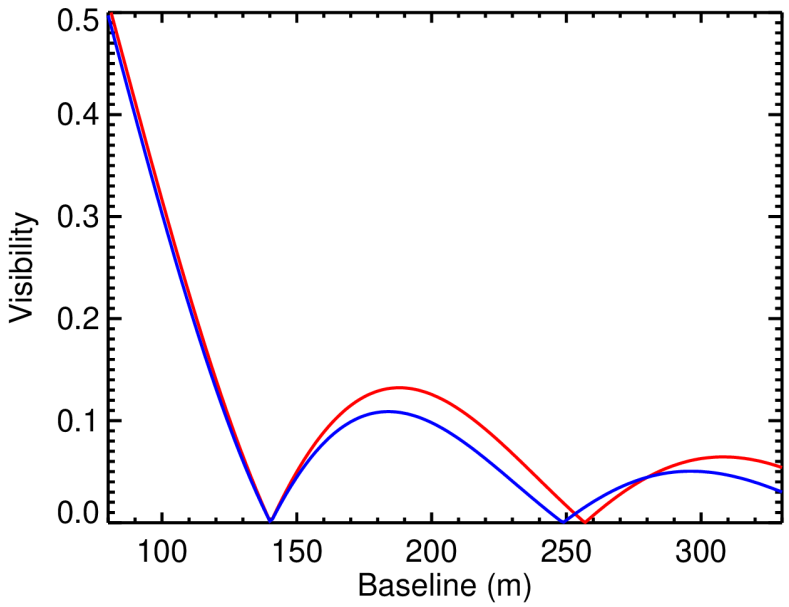

Figure 2-6: Comparison of visibility curves for a single star modeled as both a uniform disk (blue line) and as a limb-darkened disk (red line). The difference between the curves for the LDD and UDD are greater after the visibility first hits zero. Taken from "Basics of Interferometry."

While the effects of the LDD are less obvious in the first lobe of the graph, where information about the angular diameter is encoded, the LDD must still be taken into account to ensure an accurate measurement.

2.2.5 How Angular Diameter Measurements Lead to Stellar Radius

The physical stellar radius of the star is of more interest than its angular size on the sky. If the distance to the star is known, its radius can be determined from the angular diameter using trigonometry.

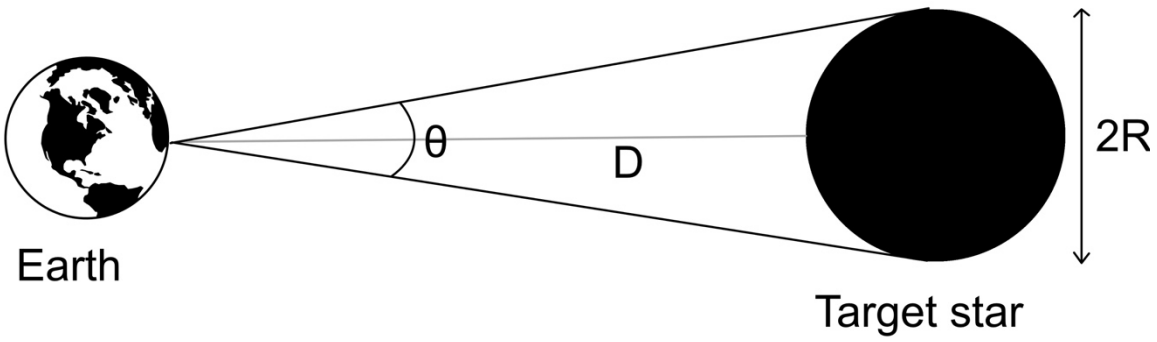

Figure 2-7: Author's rendition of the relationship between angular diameter θ and physical stellar radius R. D represents the distance to the target star from Earth.

Because the distances to stars are so large relative to their angular diameters, it is possible to use small-angle approximation to determine radii, leading to the below equation. R refers to the physical stellar radius, D refers to the distance from Earth to the star, and θ refers to the angular diameter of the star. Note that θ must be converted to radians for this to work.

$$R = \frac{\theta D}{2}$$

Aside from the directly-measured angular diameter, the only other quantity this equation relies upon is the distance to the star. Distances to nearby stars can be inferred accurately using stellar parallax — that is, measuring the shift of a star relative to the background stars at different points in Earth's orbit. The stars studied in this thesis all have parallax distance errors under 4%, and most of them are far below that threshold.

2.3 The Role of Calibrator Stars in Observational Astronomy

Before moving on from the observational background, it is important to mention calibrator stars, which are key to the procedures outlined in Chapter 3. Calibrators, also known as standard stars,

are bright, nearby, unresolved stars with well-known parameters. Alternating between the target star and calibrator stars helps account for atmospheric conditions on the night of the observation. If the calibrator star looks dimmer than it actually is, for example, then the target star must look dimmer than reality as well.

Calibrator stars come with several considerations. Stars move during the course of a night, so if the telescope loses track of a calibrator star, it becomes necessary to take extra images of the calibrator. Uneven atmospheric conditions between the calibrator star and target star may affect the results. If a calibrator cannot be properly compared to the target star, whole nights of data may be unusable. A popular way to reduce the chance of a bad calibrator is to use two calibrator stars and alternate between each. An observation sequence of this kind might go: calibrator 1, target, calibrator 2, target, calibrator 1, target, calibrator 2, target, calibrator 1, etc. Nonetheless, if it becomes apparent that a calibrator is not working correctly during the course of a night, it may be necessary to switch it out for another calibrator.

2.4 What Are Retired A Stars?

Stars are often classified according to a graph that plots temperature against luminosity, known as a Herzsprung-Russell Diagram or H-R Diagram.

As shown in Figure 2-8, stars of different temperatures are classified according to a letter-based system. From hottest to coolest, these spectral types are O, B, A, F, G, K, and M. Stars can be further classified with a number from 0-9 following the letter, with 0 indicating the hottest star of its type and 9 being the coolest. The Sun, which is considered a medium-sized star and is quite hot for its spectral type, is classified as a G2 star. A-type stars are relatively massive, usually between 1.4 and 2.1 times the mass of our Sun (Habets and Heintze, 1981).

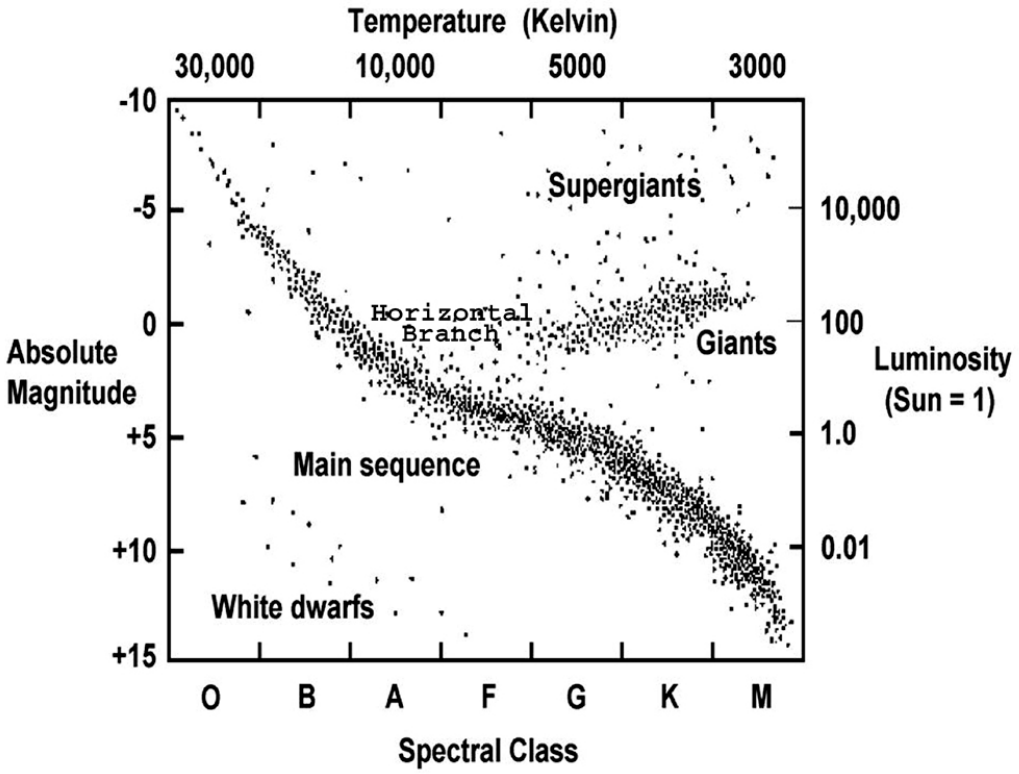

Figure 2-8: An H-R diagram plots a star's temperature against its luminosity. Taken from "Pulsating Variable Stars and the Hertzsprung-Russell Diagram."

The diagonal band cutting through the center of the H-R diagram is known as the main sequence. Stars in this population are stable, fueled by fusing hydrogen into helium in their cores. O-type stars may remain in this stage of life for a few million years, while M-type stars may remain on the main sequence for a trillion years. A Roman numeral luminosity class is often added to spectral types to indicate the life stage of a star, with class V indicating a main-sequence star.

When a star has used up all the hydrogen in its core, a second layer of hydrogen ignites around the now-inert helium core. The conditions in the core are not extreme enough to start fusing the helium yet, but the star begins to puff up into a subgiant and become cooler. Stars of

this kind are given the luminosity class IV, though the difference between a subgiant of luminosity class IV and a giant of luminosity class III are not always clear-cut. A-type stars in this stage of their evolution are known as “retired A stars.”

2.5 The Doppler Spectroscopy Method of Exoplanet Detection

Detection of exoplanets may involve Doppler spectroscopy, transits, direct observation and gravitational microlensing (Fischer et al., 2014). Doppler spectroscopy is the second-most fruitful technique, after transit observations, with over 1,000 exoplanets discovered to date with this method (“Exoplanet and Candidate Statistics”).

Doppler spectroscopy, also known as the radial velocity method, involves precisely measuring the radial velocity of a star for wobbles that might indicate the presence of an exoplanet (Wright and Gaudi, 2012). It works best with large planets and planets that orbit close to their stars, factors which both make the wobbles more pronounced (Fischer et al., 2014).

Main-sequence A-type stars often rotate so fast that the Doppler spectroscopy method does not provide clear results. However, former A stars that have progressed to the subgiant stage rotate more slowly, making Doppler spectroscopy a feasible way of detecting exoplanets around them (Johnson et al., 2007).

To detect smaller planets and planets that orbit further from their host stars, noise from the host star is modelled to avoid confusing it for velocity shifts due to an exoplanet (Fischer et al., 2014). These models require high-quality measurements of star properties.

When a planet is discovered with Doppler spectroscopy, its minimum mass may be found from the radial velocity semi-amplitude, but only if the mass of the star is also known (Fischer et al., 2014). The orbital inclination of the planet affects how closely the minimum mass

approaches the actual planetary mass, but there is an 87% chance that the actual mass is less than twice the minimum mass (Fischer et al., 2014). This is an example of information about exoplanets that researchers may obtain by having accurate measurements for the host star.

2.6 Planet Formation, Star Mass, and the Malmquist Bias

Not all types of stars appear equally likely to form all types of planets. For example, planets seem more likely to occur around stars with a higher metallicity (Wang and Fischer, 2014). There is a more tenuous correlation between star mass and planet occurrence. For example, stars of the spectral type M have significantly fewer large planets than F-type, G-type, or K-type stars (Mulders et al., 2015). Main-sequence M-type stars have lower masses than FGK types, suggesting a relationship between the formation of giant planets and stellar mass.

Research on subgiants like retired A stars suggests that the occurrence of giant planets increases with star mass (Ghezzi et al., 2018). However, these results are complicated by the so-called "retired A star mass controversy," which cast doubt on the accuracy of retired A star mass measurements. This is further discussed in section 2.7.

Statistical biases may affect perceptions of the relationship between star mass and planet formation. The Malmquist bias refers to a selection effect where readily-available astronomical data are not representative of the population (Teerikorpi, 1997). While originally coined to refer to cosmological problems, the Malmquist bias also usefully describes star population selection biases. More luminous stars can be seen at larger distances from Earth, so proportionally more of them can be observed. Similarly, binary star systems have a higher combined luminosity than a single star, and are therefore overrepresented in the pool of observable stars (Bouma et al.,

2018). This effect may have ramifications for perceptions about how exoplanets are distributed among stars of different masses.

Another bias comes from the types of stars observed by exoplanet missions. NASA's Kepler space telescope, which retired in 2018, uncovered the most confirmed exoplanets of any mission to date ("Exoplanet and Candidate Statistics"). Kepler's mission was to find Earth-like planets, so its targets were typically stars comparable to our Sun — G-type stars on or near the main sequence (Batalha et al., 2010). In general, mid-mass main sequence stars are the most commonly investigated planet host candidates, because higher-mass stars rotate too fast for Doppler spectroscopy and lower-mass stars are often too faint to be observed (Muirhead et al., 2011). This means retired A stars are an area of potential in terms of exoplanet investigation.

2.7 The Retired A Star Mass Controversy

A problem with relating retired A star masses to planetary formation is that some of their mass measurements may not be accurate. This means that other types of stars might be misclassified as retired A stars, jeopardizing research into the relationship between planet formation and star mass.

One method used to measure the mass of a star is observing the target star using spectroscopy and comparing the results to models of theoretical spectra with known masses to find a mass that best fits the observed spectrum (Malla et al., 2020). For giant stars such as retired A stars, it is not always clear which model to use due to large error boxes (Malla et al., 2020). This led to some research suggesting that retired A star masses had been overestimated, and that many supposed retired A stars were retired F or G stars instead (Lloyd, 2011).

Researchers attempted to resolve the controversy by measuring retired A star candidate masses using multiple methods. Malla et al. (2020) found that retired A star mass estimates obtained from spectroscopy had likely been overestimated, but only for stars above 1.6 solar masses. Stars miscategorized as retired A stars are likely few in number. These results also mean that giant planet occurrence increases with retired A star mass even more steeply than previously thought (Malla et al., 2020).

Due to this past systemic error in measurements of retired A star masses, it becomes more crucial to test the models for retired A star properties to ensure accurate results. Chapter 3 will discuss the methods used in this thesis to attempt a disruption of existing models.

2.8 References

"Basics of Interferometry." Center for High Angular Resolution Astronomy, Georgia State University. https://www.chara.gsu.edu/public/basics-of-interferometry

Batalha, Natalie M., et al. "Selection, Prioritization, and Characteristics of Kepler Target Stars." *The Astrophysical Journal* 713. 2(2010): L109–L114.

Bouma, L.G., et al. "Biases in Planet Occurrence Caused by Unresolved Binaries in Transit Surveys." The Astronomical Journal, Volume 155, Number 6 (2018)

Chromey, Frederick R. "To Measure the Sky: An Introduction to Observational Astronomy," second ed. Cambridge University Press, 2016.

"Exoplanet and Candidate Statistics." NASA Exoplanet Archive. https://exoplanetarchive.ipac.caltech.edu/docs/counts_detail.html

Fischer, Debra A., et al. “Exoplanet detection techniques.” In *Protostars and Planets VI*, ed. Henrik Beuther, Ralf S. Klessen, Cornelis P. Dullemond, and Thomas Henning, University of Arizona Press, 2014, pp. 715–737

Ghezzi, Luan, et al. “Retired A Stars Revisited: An Updated Giant Planet Occurrence Rate as a Function of Stellar Metallicity and Mass.” The Astrophysical Journal, Volume 860, Number 2 (2018)

Habets, G. M. H. J., and J. R. W. Heintze. “Empirical bolometric corrections for the main sequence.” Astronomy and Astrophysics, Suppl. Ser., Vol. 46, p. 193-237 (1981)

Johnson, John Asher et al. “Retired A Stars and Their Companions: Exoplanets Orbiting Three Intermediate-Mass Subgiants.” The Astrophysical Journal, Volume 665, Number 1. August 10, 2007.

Lloyd, James P. “‘Retired’ Planet Hosts: Not So Massive, Maybe Just Portly After Lunch.” The Astrophysical Journal Letters, Volume 739, Number 2 (2011)

Malla, Sai Prathyusha et al. “Asteroseismic masses of four evolved planet-hosting stars using SONG and TESS: resolving the retired A-star mass controversy,” *Monthly Notices of the Royal Astronomical Society*, Volume 496, Issue 4, August 2020

Mucciarelli, A., et al. “Exploiting the Gaia EDR3 photometry to derive stellar temperatures.” A&A Volume 653, September 2021.

Muirhead, Philip S., et al. “Precise Stellar Radial Velocities of an M Dwarf with a Michelson Interferometer and a Medium-Resolution Near-Infrared Spectrograph.” Publications of the Astronomical Society of the Pacific, Volume 123, Number 904 (2011)

Mulders, Gijs D., et al. “An Increase in the Mass of Planetary Systems Around Lower-Mass Stars.” The Astrophysical Journal, Vol. 814, No. 2 (2015)

"Pulsating Variable Stars and the Hertzsprung-Russell Diagram." Chandra X-Ray Observatory.

Teerikorpi, P. "Observational Selection Bias Affecting the Determination of the Extragalactic Distance Scale." Annual Review of Astronomy and Astrophysics, Vol. 35:101-136, Sept. 1997.

Wang, Ji, and Debra A. Fischer. "Revealing a Universal Planet-Metallicity Correlation For Planets of Different Sizes Around Solar-Type Stars." The Astronomical Journal, Volume 149, Number 1 (2014).

Wright, Jason T., and B. Scott Gaudi. "Exoplanet detection methods." *arXiv preprint arXiv:1210.2471* (2012).

3 METHODS

This chapter begins with a brief overview of the CHARA array and some details about the five retired A stars in the sample. The discussion moves on to the reduction and calibration of the raw data using CHARA's Redfluor and Calibir software packages. Finally, the chapter covers the processes used to fit and model the data to find the radius, luminosity, effective temperature, mass, and age of the target stars.

3.1 The Observatory

The CHARA array consists of six one-meter telescopes arranged in a Y shape (Figure 3-1). The arms of the Y shape are referred to as the East, West, and South arms, with two telescopes on each arm. Each telescope is a one-meter Mersenne-type afocal beam reducer ("The CHARA Array"). Several combinations of telescopes may be used to create interference fringes, allowing for 15 possible observation baselines of anywhere between 34 and 331 meters ("The CHARA Array").

For this project, the observations came from the CLASSIC instrument, which utilizes two of CHARA's telescopes at a time. CLASSIC was the first beam combiner used at CHARA and can observe fainter stars than any other instrument in the facility ("CHARA Facility and Instruments"). At its best, CLASSIC can observe stars as faint as magnitude 8.5, and can typically achieve observations of stars at magnitude 7.0 ("Applying for Observing Time"). All of the stars in this sample are brighter than 7.0 magnitudes. Each star was observed by at least two different pairs of telescopes to ensure a variety of baselines.

The observations for this project were taken in the H-band (1.67 μm), K-band (2.13 μm), and J-band (1.3 μm). Most of the J-band observations proved to be unusable. However, there were not enough J-band observations to significantly reduce the number of samples.

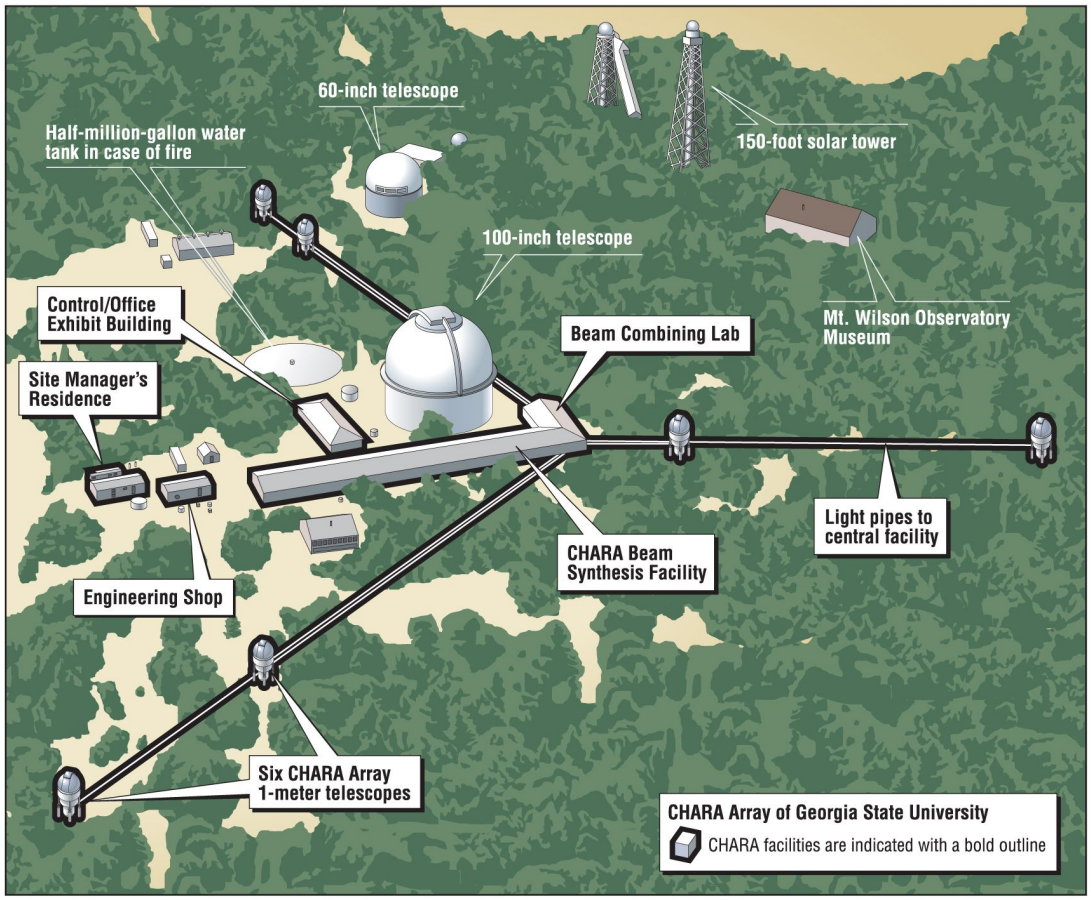

Figure 3-1: Diagram of the CHARA array.

3.2 The Target Stars

The sample for this thesis consists of five well-measured retired A stars in our stellar neighborhood. All are within 100 parsecs of Earth, ensuring accurate distance measurements. The stars were all observed with CHARA's CLASSIC instrument several times between the years 2008 and 2019.

3.2.1 HD22713

Located in the constellation of Eridanus, HD22713 (Figure 3-2) is considered a high proper motion star with the spectral type K0 IV, indicating that it is a subgiant and among the hottest K-type stars ("HD22713"). Proper motion refers to the apparent angular velocity of a star as observed from our solar system (Koupelis and Kuhn, 369). All stars have some level of proper motion, but the closest stars have the most noticeable levels, and are referred to as high proper motion stars (Koupelis and Kuhn, 369).

HD22713 is one of our nearest stellar neighbors, and it is the closest star to Earth in this sample, lying about 35 parsecs away (Bailer-Jones et al., 2021). The star has an apparent V-band magnitude of 5.96, making it visible with the naked eye on a clear, dark night ("HD22713").

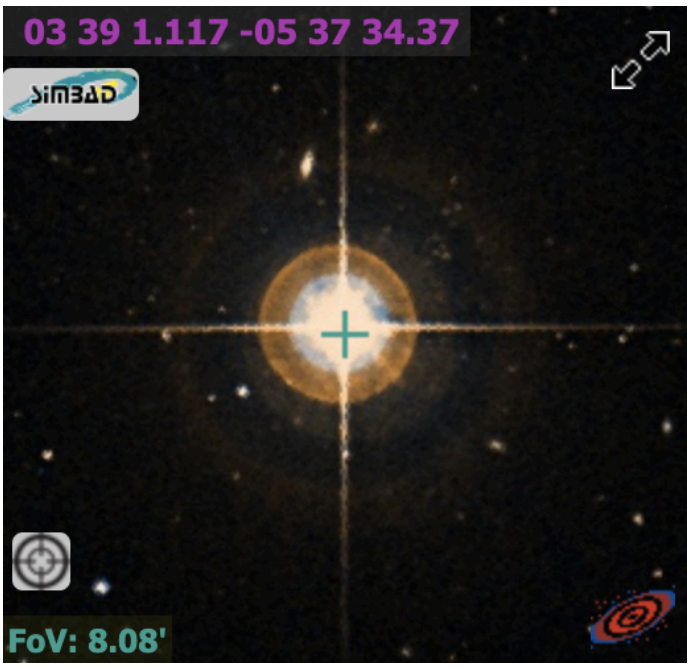

Figure 3-2: HD22713 as imaged by the Digitized Sky Survey. Picture retrieved from SIMBAD Astronomical Database, http://simbad.cds.unistra.fr/simbad/sim-id?Ident=HD22713.

3.2.2 HD37601

HD37601 (Figure 3-3) is located in the constellation of Camelopardis about 59 parsecs from Earth (Bailer-Jones et al., 2021). It has an apparent V-band magnitude of around 6, making it visible with the naked eye ("HD37601"). Like most of the other stars in this sample, HD37601 is currently a K-type star, and has the specific spectral classification K0 III ("HD37601"). While its luminosity class indicates a giant star rather than a subgiant, the exact line between giants and subgiants is not easily drawn, and it is still considered a retired A star for the purposes of this study.

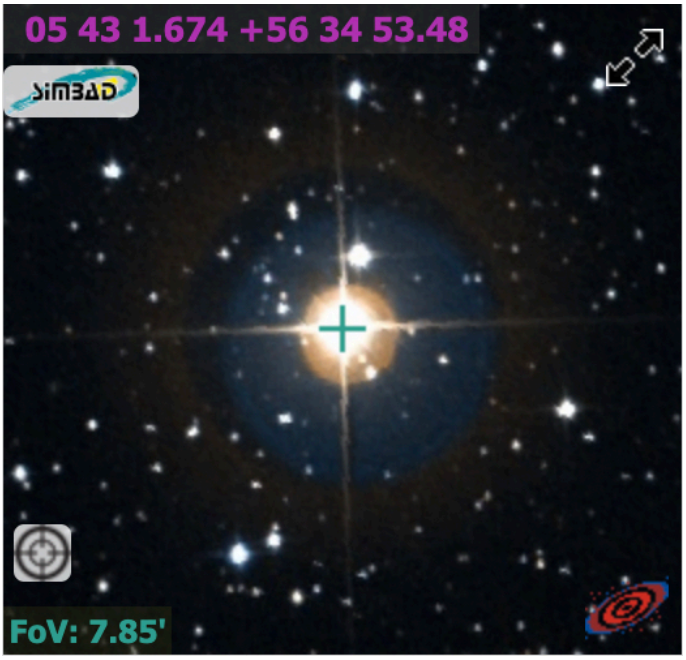

Figure 3-3: HD37601 as imaged by the Digitized Sky Survey. Picture retrieved from SIMBAD Astronomical Database, http://simbad.cds.unistra.fr/simbad/sim-id?Ident=HD37601.

3.2.3 HD45410

HD45410 (Figure 3-4) is a high proper motion star located in the constellation of Lynx around 55 parsecs from Earth (Bailer-Jones et al., 2021). A commonly-used alias for this star is 6

Lyncis. While its spectral type was previously recorded as K0.5 III (Keenan and McNeil, 1989), indicating a giant star, more recent studies have classified it as a subgiant of the type K0 IV (Sato et al., 2008). At a V-band magnitude of 5.855, HD45410 is visible from Earth with the naked eye ("HD45410").

HD45410 hosts the exoplanet HD45410b, which has an orbital period estimated as low as 875 days (Bowler et al., 2010) and as high as 934 days (Luhn et al., 2019). Its minimum mass has been estimated between 2.4 Jupiters (Sato et al., 2008) and 2.010 Jupiters (Luhn et al., 2019). The planet was discovered in 2008 via the radial velocity method (Sato et al., 2008).

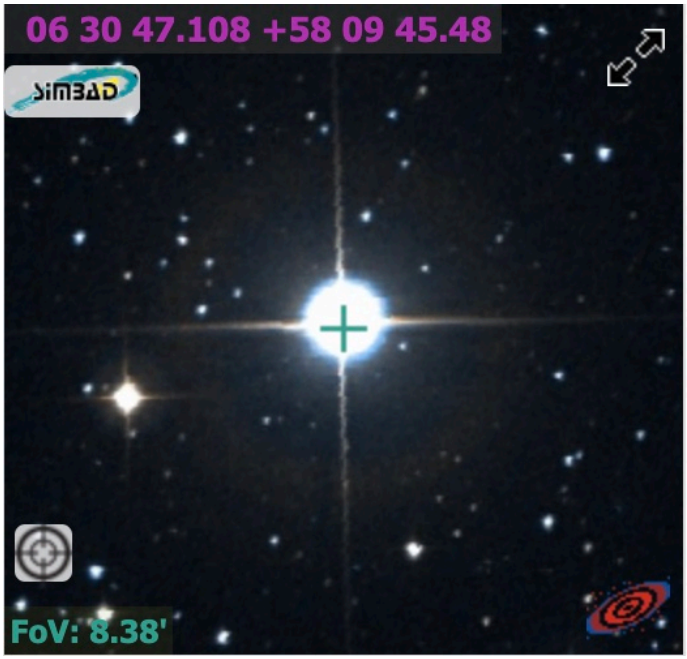

Figure 3-4: HD45410 as imaged by the Digitized Sky Survey. Picture retrieved from SIMBAD Astronomical Database, http://simbad.cds.unistra.fr/simbad/sim-id?Ident=HD45410.

3.2.4 HD200964

Found in the constellation of Equuleus, HD200964 (Figure 3-5) is the furthest star from Earth in this sample, sitting about 72 parsecs away (Bailer-Jones et al., 2021) despite being classified as a

high proper motion star (“HD200964”). It has a V-band magnitude of 6.487, too faint for most people to see with the naked eye (“HD200964”). HD200964 is the only star in the sample that is not a K-type star — its spectral type is G8 IV, making it a cool G-type subgiant (“HD200964”).

The star hosts two known exoplanets, HD200964b and HD200964c, both discovered in 2010 by the radial velocity method (Johnson et al., 2011). The minimum mass of HD200964b has been estimated as high as 2.27 Jupiters (Stassun et al., 2017) and as low as 1.6 Jupiters (Luhn et al., 2019). The minimum mass of HD200964c has been estimated at around 0.9 Jupiters (Johnson et al., 2011) and, more recently, around 1.214 Jupiters (Luhn et al., 2019).

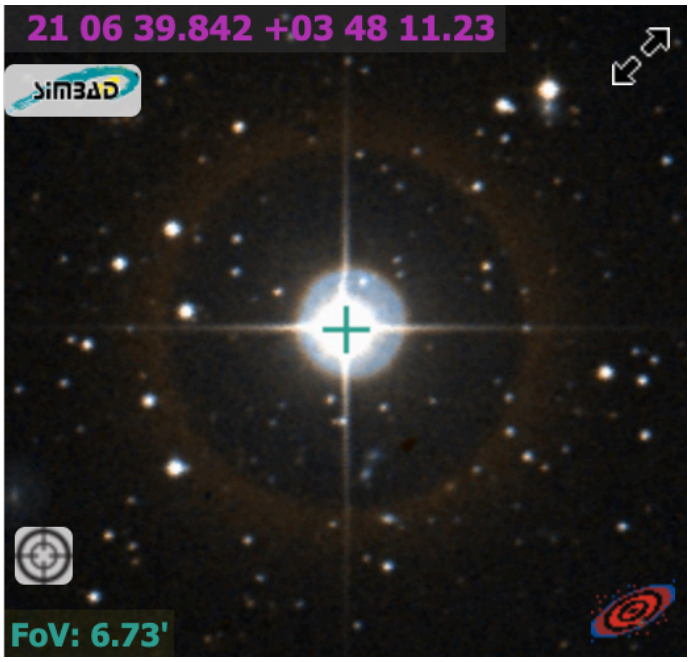

Figure 3-5: HD200964 as imaged by the Digitized Sky Survey. Picture retrieved from SIMBAD Astronomical Database, http://simbad.cds.unistra.fr/simbad/sim-id?Ident=HD200964.

3.2.5 HD210702

HD210702 (Figure 3-6) lies about 54 parsecs from Earth (Bailer-Jones et al., 2021) in the constellation of Pegasus. It has a V-band magnitude of around 5.9, making it visible with the

naked eye (“HD210702”). Some studies list HD210702 as a K0 III star (“HD210702”), which would indicate a giant star, while others consider it to be a K1 IV star (Sato et al., 2012), which would indicate a subgiant.

In 2007, the radial velocity method revealed the existence of this star’s companion HD210702b (Johnson et al., 2007). The exoplanet has a minimum mass of around 1.9 times that of Jupiter and an orbital period of 354 days (Sato et al., 2012).

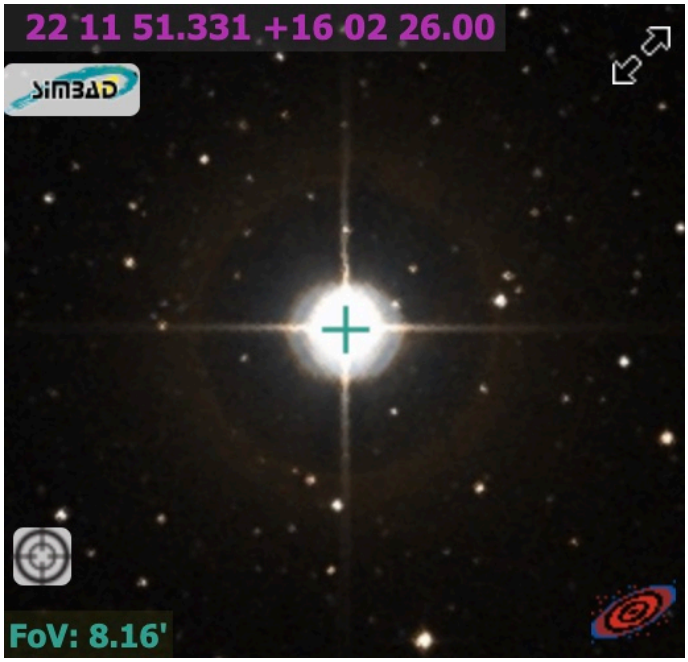

Figure 3-6: HD210702 as imaged by the Digitized Sky Survey. Picture retrieved from SIMBAD Astronomical Database, http://simbad.cds.unistra.fr/simbad/sim-id?Ident=HD210702.

3.2.6 Eliminated star: HD215549

Retired A star HD215549 was originally part of the sample suite. However, stellar model fitting for the age of this star (discussed in Section 3.6) showed the star to be older than the universe, suggesting an error in the data. A bad calibrator star was hypothesized to be the source of the error, but the exact culprit could not be identified, so HD215549 was removed from the sample.

3.3 The Calibrator Stars

Like all observational methods, interferometry requires the use of calibrator stars to ensure accurate measurements, as discussed in section 2.3.

Table 3-1 shows all the calibrator stars used in the data sample for this thesis, along with the target stars they were matched with. Not all of the calibrators were used on the same night; for the most part, some combination of two calibrator stars was used.

Target Star	**Calibrator Stars**
HD 22713	HD 21790, HD 20395
HD 37601	HD 39283, HD 43378, HD 46317, HD 36066
HD 45410	HD 46590, HD 39283, HD 43378, HD 46317, HD38091
HD 200964	HD201507, HD203562, HD203521, HD204121, HD203843
HD 210702	HD210074, HD206043, HD207223, HD209166, HD196180

Table 3-1 Target stars and their calibrators

3.4 The Data Reduction Process

Data reduction for each raw target-star and calibrator-star observation was performed using CHARA's Redfluor utility. Redfluor compiled the data into raw squared visibilities that could be calibrated in the next phase.

Figure 3-7 shows a waterfall plot produced by Redfluor of interference fringes for a high-quality observation of the target star HD37601. The vertical axis represents time, and the horizontal axis represents the optical path difference between the two telescopes. The clear definition of the waterfall plot, with the fringes mostly confined to a strip down the middle of the

graph, is a sign that the observation was not hindered by much atmospheric turbulence or other disturbances.

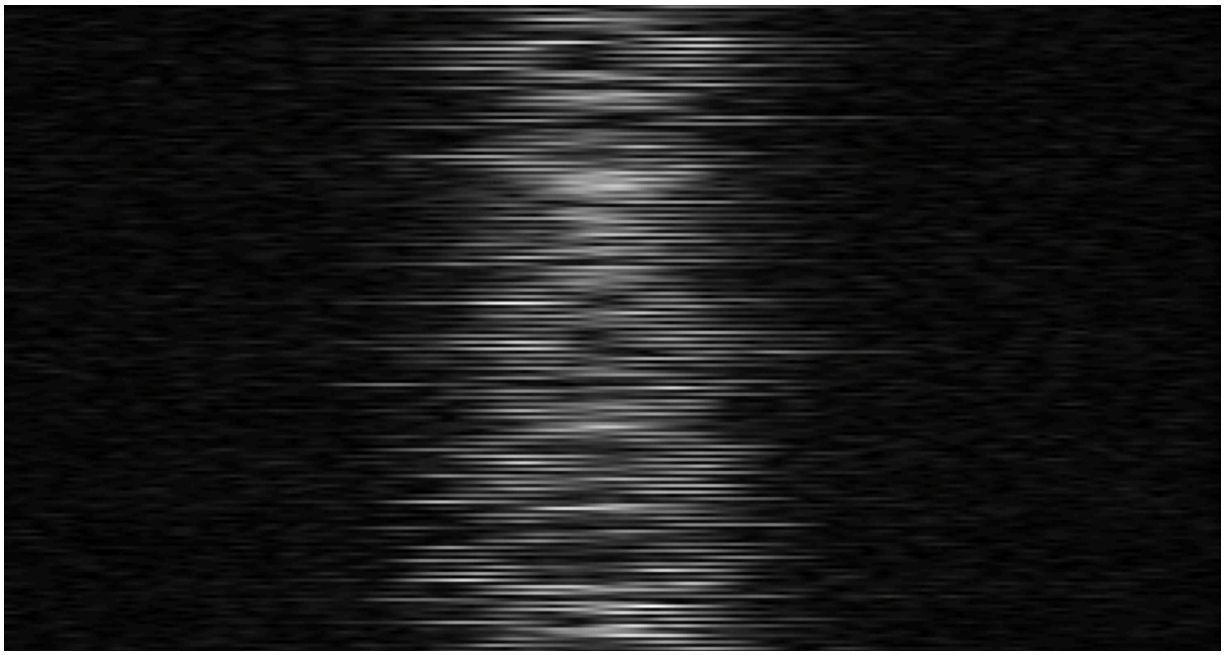

Figure 3-7: Waterfall plot from Redfluor of an observation of HD37601 taken by CHARA on December 18, 2015.

Redfluor subtracts the background noise from the observation to leave only the raw visibility of the star. The sky itself is not completely dark, due to light diffusion from other stars, and it is necessary to subtract this background light to get accurate measurements of the target star. Noise may also be caused by the electricity running through the instrument itself.

Figure 3-8 shows graphs for the photometry and power spectra for an observation of HD37601 before and after subtracting the background noise. In this case, there was not much noise to subtract, but Redfluor still eliminated the small amount of noise effectively. The upper two diagrams show the photometry, or flux from the starlight, on the y axis, and the scan number (a proxy for time) on the x axis. Note the different colors for the photometry from different telescopes.

The lower two diagrams show the power signal on the y axis and the frequency in Hertz on the x axis. Ideally, the two telescope signals should peak close together, as they do in this example.

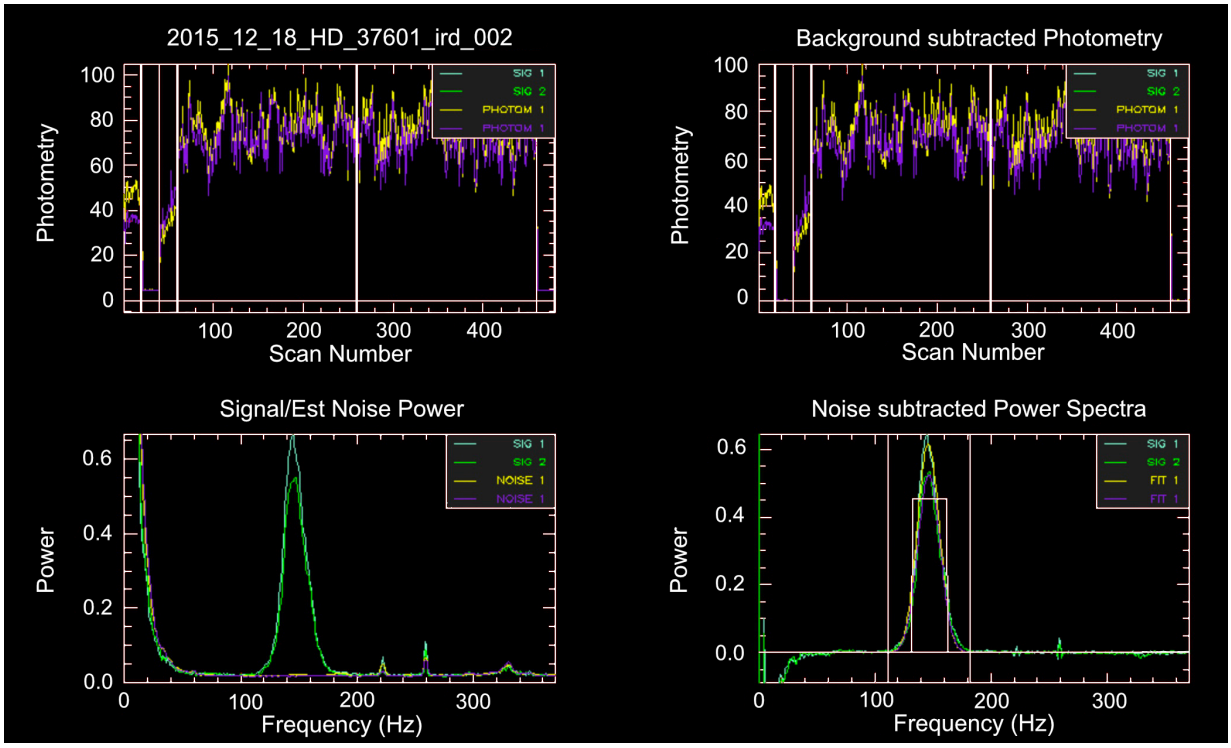

Figure 3-8: Photometry and power spectra graphs from Redfluor for a CHARA observation of HD37601 on December 18, 2015.

After raw visibilities were obtained for each target star observation and calibrator star observation, the next step was to calibrate the visibilities.

3.5 Data Calibration

The raw visibilities for each night of data were bundled together and calibrated using CHARA's Calibir package. The process required inputs for the known angular diameters and errors of the calibrator stars, which were obtained from Bourges et al. (2017). This allowed the software to

calculate the adjustment needed to turn the raw calibrator star visibilities into their proper visibilities, and in turn perform that same adjustment to the target star raw visibility.

Figure 3-9 shows a Calibir graph of a night of observations for target star HD45410. The y axis represents visibility squared, with 0 being completely resolved and 1 being a completely unresolved point source. The x axis represents time in hours. The red dots on the graph represent the raw squared visibilities for the target star observations, and the yellow dots represent the calibrated visibilities for the target star. The green and blue dots represent the calibrated visibilities for the two calibrator stars used on the night.

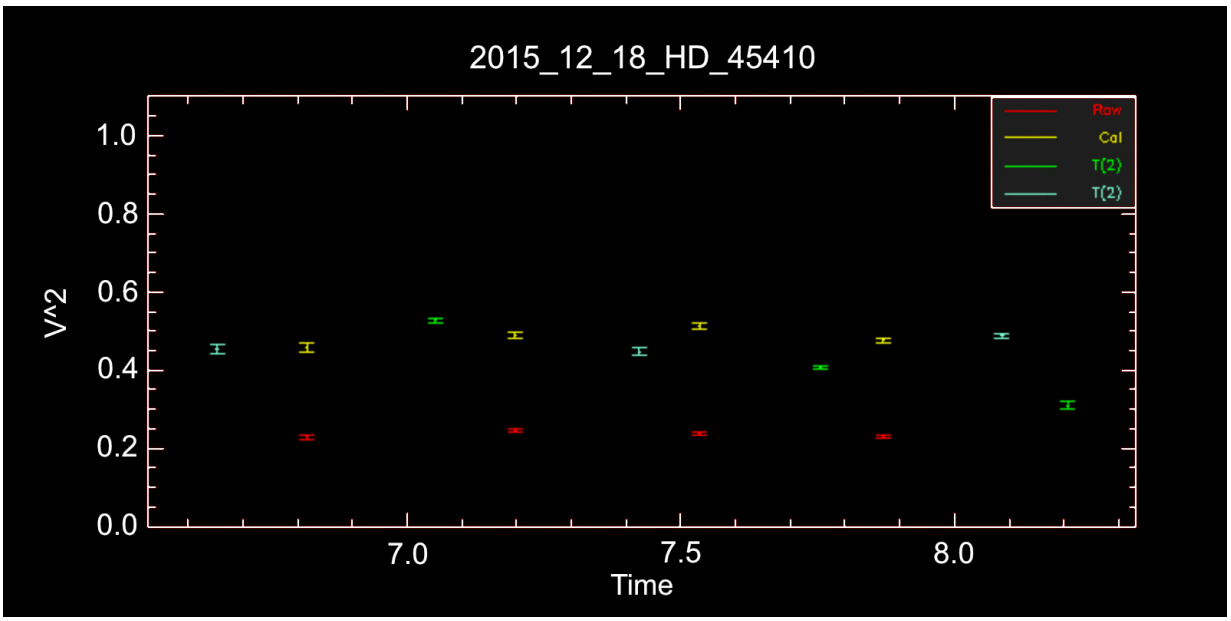

Figure 3-9: Calibir example showing each observation on the night of 12-18-2015. The target was HD45410, with raw visibilities shown in red and calibrated visibilities shown in yellow. The green and blue data points represent the calibrator stars HD39283 and HD46317.

Calibir allows for calibrating visibilities using either the mean or the median power spectra. Calibrated files were produced using both the mean and the median so that the best option to use could be determined in the fitting phase.

3.6 Fitting for Radius, Luminosity, and Effective Temperature

When each night of data had been processed by Calibir, the files were then fed into the v2fit code created by Tyler Ellis. The code provides results for the angular diameter in milli-arcseconds, radius in solar radii, luminosity in solar luminosities, effective temperature in Kelvin, and distance from Earth in parsecs for each star. Aside from the calibrated data, the required inputs are the stars' metallicity, logarithm of surface gravity, parallax angle, and bolometric flux. For this project, metallicity and surface gravity were obtained from Brewer et al. (2016), except in the case of HD22713, where the values were taken from Luck (2017). The bolometric fluxes were obtained through a private communication with Kaspar von Braun (Table 3-2), and the parallax angles were taken from van Leeuwen (2007).

Star	Bolometric flux (1e-8)	Error (1e-8)
HD22713	13.3	0.069
HD37601	12.4	0.08
HD45410	14.3	0.06
HD200964	8.38	0.059
HD210702	13.65	0.09

Table 3-2: Bolometric fluxes and errors from Kaspar von Braun

The parallax angle is necessary for calculating the distance to each star, which allows for a physical radius measurement. Bolometric flux is necessary for finding the effective temperature and luminosity of the stars. Metallicity and surface gravity are used in the correction for the LDD.

Each of the desired stellar parameters is calculated multiple times with randomized errors, and the relative frequency of these results is plotted on a bar graph. If all goes well, these graphs

appear as a normal distribution with the most commonly occurring value at the peak in the middle.

The fit was run using parallax angles from both the Hipparcos and Gaia missions as inputs. The fit was also run using the mean and the median of the power spectra, resulting in a total of four fits for each star (Hipparcos and mean, Hipparcos and median, Gaia and mean, and Gaia and median).

Gaia parallax angles have many significant figures, so the final results use the Hipparcos parallaxes to be on the safe side. Additionally, the mean and median power spectra were different enough to necessitate picking one, so because neither seemed to uniformly result in a better fit, the mean was arbitrarily chosen for subsequent use. Results in Chapter 4 reflect fits created with Hipparcos parallax angles and the mean power spectra.

3.7 Fitting for Mass and Age

The Python stellar model grid interpolation utility Kīauhōkū (Claytor et al., 2020) was used to estimate the mass and age of the target stars. Data were run through four different models: the Yale Rotating Stellar Evolution Code, aka YREC (Demarque et al., 2008), Harvard University's MESA Isochrones and Stellar Tracks, aka MIST (Dotter, 2016; Choi et al., 2016), the Dartmouth Stellar Evolution Database (Dotter et al., 2008), and the Garching Stellar Evolution Code, aka GARSTEC (Weiss and Schlattl, 2008). The mean of the results from the four models was used for the masses and ages of the target stars.

The input values required by Kīauhōkū are luminosity, temperature, and metallicity, the former two of which came from the v2fit script. To match the inputs to the synthetic star data, Kīauhōkū sometimes needs to adjust the inputs slightly, but keeps as close as possible to the

original values. The mass output from Kīauhōkū is given in solar masses, and the age output is given in gigayears, abbreviated to Gyr (one gigayear is equal to one billion years).

3.8 References

"Applying for Observing Time." Center for High Angular Resolution Astronomy, Georgia State University. https://www.chara.gsu.edu/observers/applying-for-chara-time

Bailer-Jones, C. A. L., et al. "Estimating Distances from Parallaxes. V. Geometric and Photogeometric Distances to 1.47 Billion Stars in Gaia Early Data Release 3." The Astronomical Journal, Volume 161, Issue 3, id.147 (March 2021).

Bourges, L., et al. "JMMC Stellar Diameters Catalogue - JSDC. Version 2." VizieR On-line Data Catalog: II/346 (January 2017).

Bowler, Brendan P., et al. "Retired A Stars and Their Companions. III. Comparing the Mass-Period Distributions of Planets Around A-Type Stars and Sun-Like Stars." The Astrophysical Journal, Volume 709, Issue 1 (2010)

Brewer, John M., et al. "Spectral Properties of Cool Stars: Extended Abundance Analysis of 1,617 Planet-search Stars." The Astrophysical Journal Supplement Series, Volume 225, Issue 2, article id. 32 (2016).

"The CHARA Array." Center for High Angular Resolution Astronomy, Georgia State University. https://www.chara.gsu.edu/instrumentation/chara-array

"CHARA Facility and Instruments." Center for High Angular Resolution Astronomy, Georgia State University. https://www.chara.gsu.edu/public/instrumentation

Choi, Jieun, et al. "Mesa Isochrones and Stellar Tracks (MIST). I. Solar-scaled Models." The Astrophysical Journal, Volume 823, Issue 2, article id. 102 (2016).

Claytor, Zachary R., et al. “Chemical Evolution in the Milky Way: Rotation-based Ages for APOGEE-Kepler Cool Dwarf Stars.” The Astrophysical Journal, Volume 888, Issue 1, article id. 43 (2020)

Demarque, P., et al. “YREC: The Yale Rotating Stellar Evolution Code.” Astrophysics and Space Science, Volume 316, Issue 1-4 (2008).

Dotter, Aaron. “MESA Isochrones and Stellar Tracks (MIST) 0: Methods for the Construction of Stellar Isochrones.” The Astrophysical Journal Supplement Series, Volume 222, Issue 1, article id. 8 (2016).

Dotter, Aaron, et al. “The Dartmouth Stellar Evolution Database.” The Astrophysical Journal Supplement Series, Volume 178, Issue 1, pp. 89-101 (2008).

Keenan, Philip C., and Raymond C. McNeil. “The Perkins Catalog of Revised MK Types for the Cooler Stars.” Astrophysical Journal Supplement v.71, p.245 (October 1989).

Koupelis, Theo, and Karl F. Kuhn. *In Quest of the Universe*. Jones and Bartlett Publishers, 2007.

Luck, R. Earle. “Abundances in the Local Region II: F, G, and K Dwarfs and Subgiants.” The Astronomical Journal, Volume 153, Issue 1, article id. 21 (2017).

Luhn, Jacob K., et al. “Retired A Stars and Their Companions. VIII. 15 New Planetary Signals around Subgiants and Transit Parameters for California Planet Search Planets with Subgiant Hosts.” The Astronomical Journal, Volume 157, Issue 4, article id. 149 (April 2019).

MIST models: Dotter (2016), Choi et al. (2016), and Paxton et al. (2011, 2013, 2015)

“HD200964.” SIMBAD Astronomical Database, Centre De Données Astronomiques De Strasbourg, http://simbad.cds.unistra.fr/simbad/sim-id?Ident=HD200964.

"HD210702." SIMBAD Astronomical Database, Centre De Données Astronomiques De Strasbourg, http://simbad.cds.unistra.fr/simbad/sim-id?Ident=HD210702.

"HD 210702 Overview." NASA Exoplanet Archive, NASA Exoplanet Science Institute, https://exoplanetarchive.ipac.caltech.edu/overview/HD210702

"HD22713." SIMBAD Astronomical Database, Centre De Données Astronomiques De Strasbourg, http://simbad.cds.unistra.fr/simbad/sim-id?Ident=HD22713.

"HD37601." SIMBAD Astronomical Database, Centre De Données Astronomiques De Strasbourg, http://simbad.cds.unistra.fr/simbad/sim-id?Ident=HD37601.

"HD45410." SIMBAD Astronomical Database, Centre De Données Astronomiques De Strasbourg, http://simbad.cds.unistra.fr/simbad/sim-id?Ident=HD45410.

Johnson, John Asher, et al. "Retired A Stars and Their Companions: Exoplanets Orbiting Three Intermediate-Mass Subgiants." The Astrophysical Journal, Volume 665, Issue 1 (August 2007).

Johnson, John Asher, et al. "Retired A Stars and Their Companions. VI. A Pair of Interacting Exoplanet Pairs Around the Subgiants 24 Sextanis and HD 200964." The Astronomical Journal, Volume 141, Issue 1, article id. 16 (January 2011).

Stassun, Keivan G., et al. "Accurate Empirical Radii and Masses of Planets and Their Host Stars with Gaia Parallaxes." The Astronomical Journal, Volume 153, Issue 3, article id. 136 (March 2017).

Sato, Bun'ei, et al. "Planetary Companions to Evolved Intermediate-Mass Stars: 14 Andromedae, 81 Ceti, 6 Lyncis, and HD 167042." *Publications of the Astronomical Society of Japan*, Volume 60, Issue 6, 25 December, 2008.

Sato, Bun'ei, et al. "Substellar Companions to Seven Evolved Intermediate-Mass Stars." *Publications of the Astronomical Society of Japan*, Volume 64, Issue 6, 25 December, 2012.

van Leeuwen, Floor. "Hipparcos, the New Reduction of the Raw Data." Astrophysics and Space Science Library, Volume 350. Springer Science+Business Media B.V. (2007)

Von Braun, Kaspar. Private communication, July 2022.

Weiss, Achim, and Helmut Schlattl. "GARSTEC—the Garching Stellar Evolution Code. The direct descendant of the legendary Kippenhahn code." Astrophysics and Space Science, Volume 316, Issue 1-4 (2008).

4 RESULTS

This chapter presents the results of all the methods used to calculate the parameters for each star in the sample. The v2fit code outputs values for the angular diameter, radius, luminosity, and effective temperature of each star. It also produces results for distances to the stars, but they are not discussed here because they are essentially direct functions of the parallax angle sourced from Hipparcos and not part of the literature comparison in Chapter 5. Finally, Kīauhōkū provides estimates for the mass and age of each star.

In the angular diameter fitting diagrams shown in Figures 4-1, 4-5, 4-9, 4-13, and 4-17, the left-hand pane shows visibility-squared on the y axis and spatial frequency on the x axis. Spatial frequency is equal to the foreshortened baseline divided by wavelength, and ensures that observations in different filter bands can be plotted on the same curve. The right-hand panes of the angular diameter fitting diagrams show the relative frequencies of multiple possible angular diameters with randomized errors, with the final estimated measurement appearing in the top right. Similarly, the distributions for radius, luminosity, and effective temperature represent the relative frequencies for a collection of results with randomized errors, with the final value and errors displayed in the top right.

Outputs from Kīauhōkū, including mass and age, are provided as tables. Only standard deviations were available for the mass and age estimates, and these will be used in the literature comparison in Chapter 5. It could be possible to calculate mass and age errors if each of the angular diameter values with random errors could be processed into temperature and luminosity values with v2fit and then fed into Kīauhōkū to get a mass and age measurement for each theoretical value, leading to a normal distribution of masses and ages from which errors for those

quantities could be calculated. However, this method would take an impractical amount of computing power and was therefore not feasible for this project.

The v2fit code and Kīauhōkū produced a high number of sigificant figures for radius, luminosity, mass, and age. Because the input values (for bolometric flux, surface gravity, etc.) tended to report two significant figures after the decimal point for both main values and errors, these quantities were rounded in kind.

4.1 HD22713

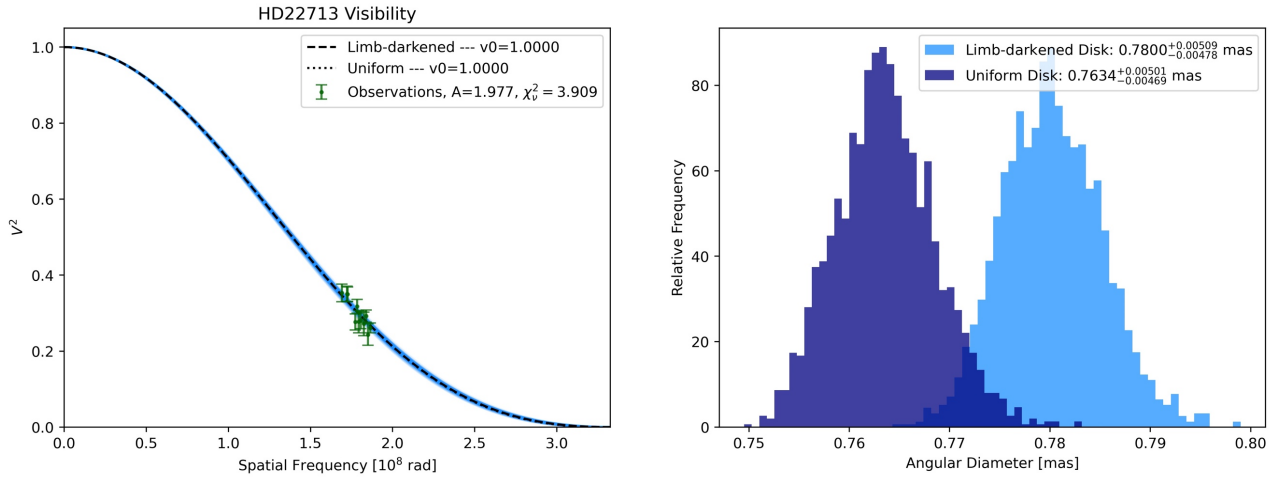

Figure 4-1: v2fit angular diameter fitting for HD22713.

There was originally a significant outlier on the fitting curve for HD22713 (Figure 4-1). However, there was an issue with the calibrator star HD20395 on one of the observation nights, so some of the target star observations were cut. It turned out one of those bad observations was the outlier, so it is not present in the final graph.

Out of all the stars, the observations for HD22713 match the closest visually with the modeled curve, with a chi-square statistic of 3.909. Its LDD came out as 0.7800 ±0.63% mas, making it the only star in the sample to have an angular diameter error of less than 1%. It has the

fewest observations of any star in the sample, so it may be that more nights of data would have created bigger errors. However, its distance error is naturally smaller than that of the other stars because it is the closest to Earth.

HD22713 is something of an outlier within the sample, with the highest effective temperature (Figure 4-3), smallest radius (Figure 4-2), and lowest luminosity (Figure 4-4) of the sample — 5061 ±0.34% Kelvin, 2.83 ±1.3% solar radii, and 4.72 ±2.5% solar luminosities respectfully. Its mass is also on the smaller side for a retired A star (Table 4-1). The high effective temperature may suggest that HD22713 is a less evolved retired A star than the others. It is unclear what the chances are of collecting a sample of five retired A stars where four are relatively similar and one is much smaller.

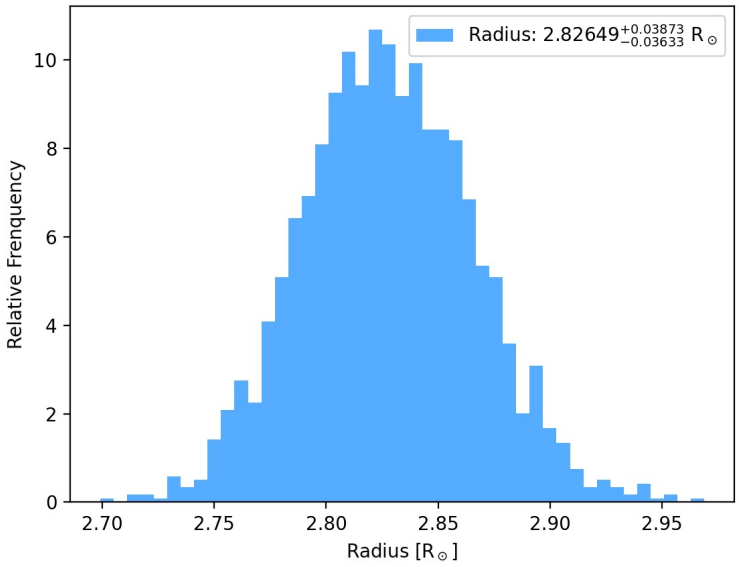

Figure 4-2: v2fit radius modeling for HD22713.

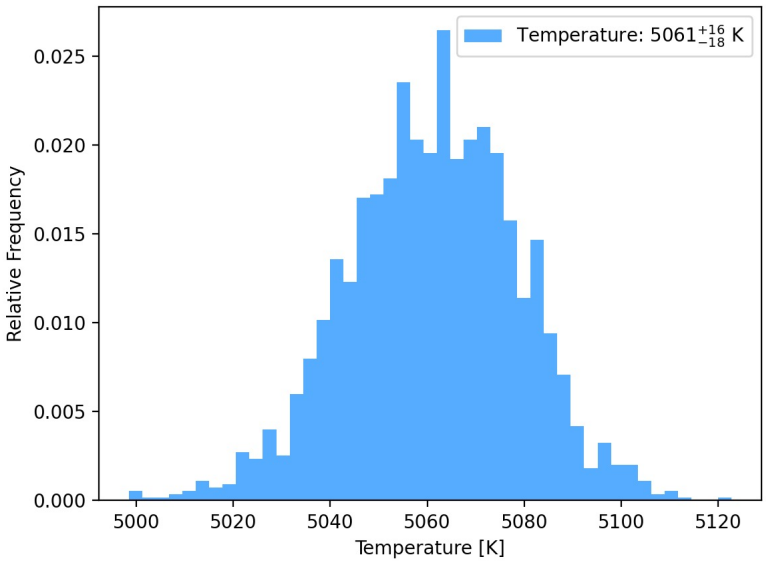

Figure 4-3: v2fit effective temperature modeling for HD22713.

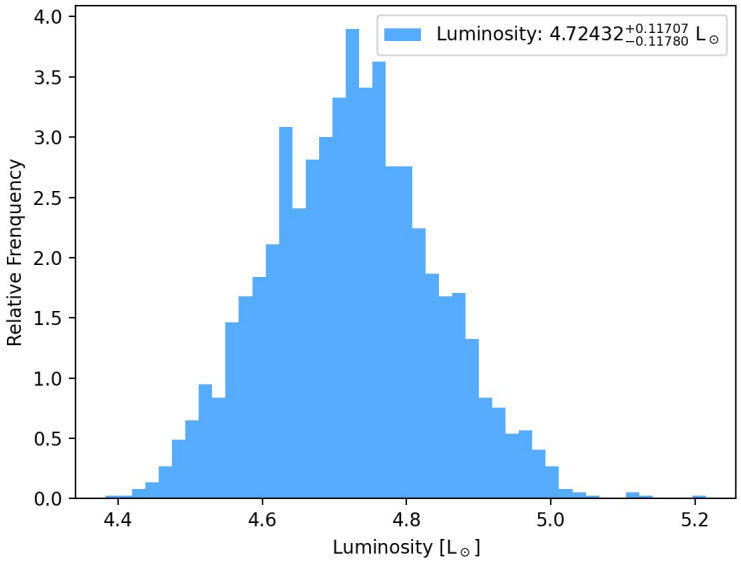

Figure 4-4: v2fit luminosity modeling for HD22713.

The ages and masses for HD22713 produced by the four different models in Kīauhōkū agree relatively closely, with the mass estimated at just above 1.29 solar masses and the age

estimated as almost 4.5 Gyr (close to the age of our Sun). It is the second-oldest star in the sample, but that does not contradict the theory that HD22713 is less evolved than the other targets — stars with a lower mass age slower than stars with a higher mass. Full Kīauhōkū results for HD22713 are displayed in Table 4-1. Note that not all figures for these outputs are significant; rounded figures are reported in Table 4-2.

	yrec	**mist**	**dartmouth**	**garstec**	**mean**	**Std dev**	**Mass offset**
initial_ mass	1.291354	1.297520	1.328375	1.264866	1.295529	2.607963e-02	6.350846e-02
initial_ met	0.030000	0.030000	0.030000	0.030000	0.030000	1.830367e-07	4.109293e-07
eep	541.815016	475.700880	539.642171	545.029279	525.546836	3.330424e+01	6.932840e+01
mass	1.291354	1.296741	1.328375	1.261736	1.294552	2.730009e-02	6.663865e-02
teff	5060.999134	5061.004262	5061.000516	5060.999933	5061.000961	2.272321e-03	5.128246e-03
lum	4.724000	4.724005	4.724000	4.724000	4.724001	2.285362e-06	4.626873e-06
met	0.030000	0.030000	0.030000	0.030000	0.030000	1.830367e-07	4.109293e-07
logg	3.645328	3.649946	3.657742	3.634836	3.646963	9.570951e-03	2.290553e-02
age	4.621465	4.211529	4.155754	4.990426	4.494794	3.902493e-01	8.346716e-01

Table 4-1: Mass and age modeling results for HD22713 from Kīauhōkū.

A summary of the measured values and errors for the characteristics of HD22713 is displayed in Table 4-2. Due to the low angular diameter and distance errors, the other star properties calculated by v2fit also have low errors. Luminosity typically has the highest error of

all the stellar characteristics from v2fit, because calculating it requires propagating the error from multiple other parameters.

	Value	**Upper error**	**Lower error**	**Mean error**	**Percent error**
Angular Diameter (mas)	0.7800	0.0051	0.0048	±0.0049	±0.63%
Radius ($R_\odot$)	2.83	0.039	0.036	±0.038	±1.3%
Effective temperature (K)	5061	16	18	±17	±0.34%
Luminosity ($L_\odot$)	4.72	0.12	0.12	±0.12	±2.5%
	Value	**Std Dev**			
Mass ($M_\odot$)	1.29	0.027	-	-	-
Age (Gyr)	4.49	0.39	-	--	

Table 4-2: Summary of measured values for HD22713

4.2 HD37601

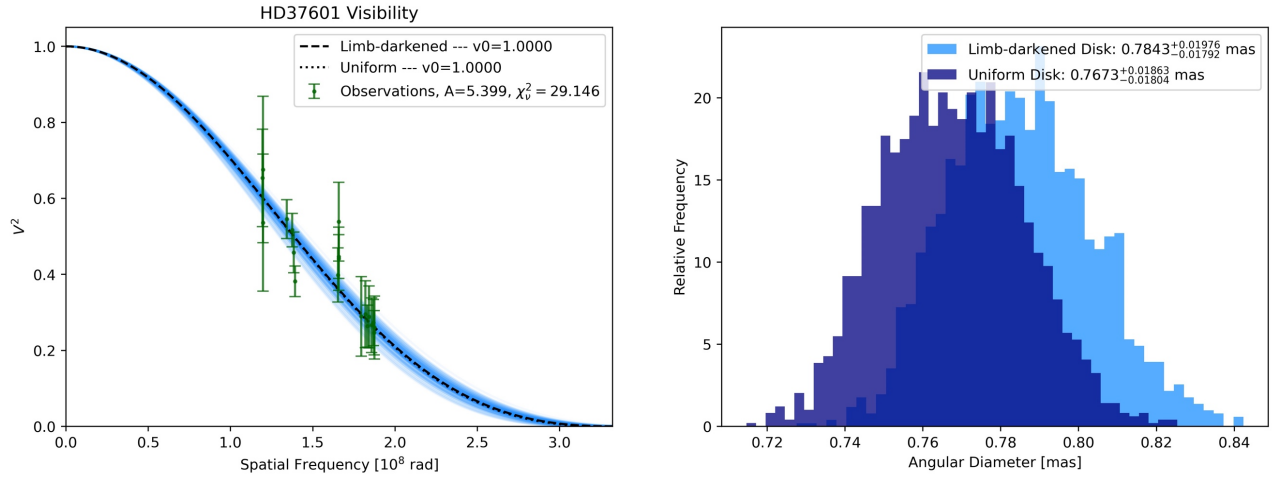

Figure 4-5: v2fit angular diameter fitting for HD37601.

Despite the large error bars in the fitting process for HD37601, and the large chi-square statistic of 29.146, the error on the angular diameter is relatively reasonable (Figure 4-5). The final LDD estimate is 0.7843 ±2.4% mas.

The radius of HD37601 is estimated as 4.99 ±3.3% solar radii (Figure 4-6). Its effective temperature comes out as 4959 ±1.2% K (Figure 4-7), and its luminosity is 13.58 ±4.7% solar luminosities (Figure 4-8).

The radii, effective temperatures, and luminosities for HD37601, HD45410 (Figures 4-10, 4-11, and 4-12), and HD200964 (Figures 4-14, 4-15, and 4-16) are quite close together. The luminosity is determined by radius and effective temperature, so agreement between these quantities is not unusual.

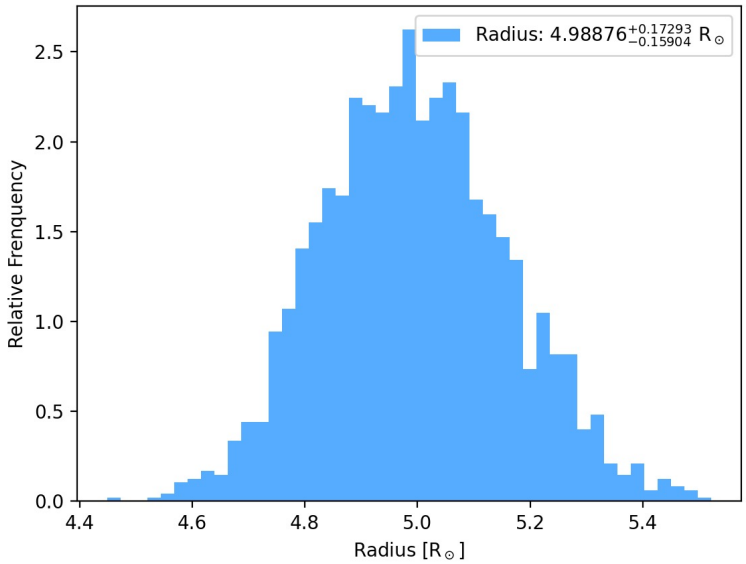

Figure 4-6: v2fit radius modeling for HD37601.

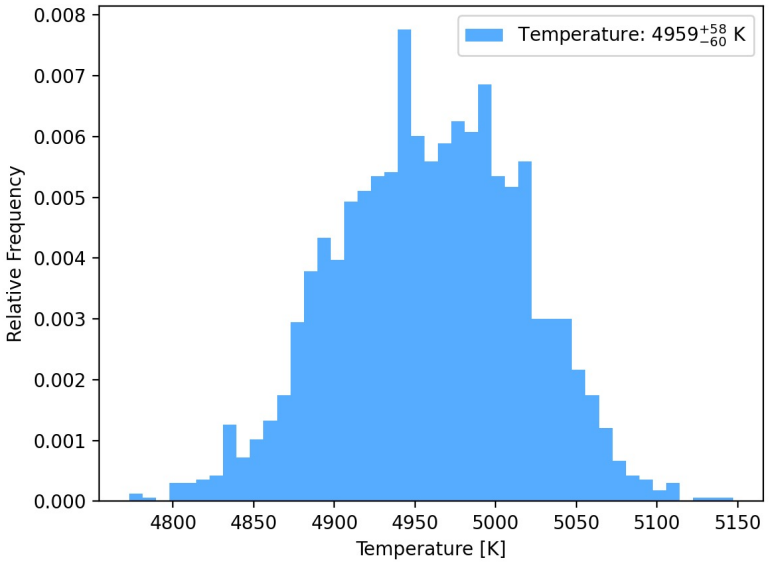

Figure 4-7: v2fit effective temperature modeling for HD37601.

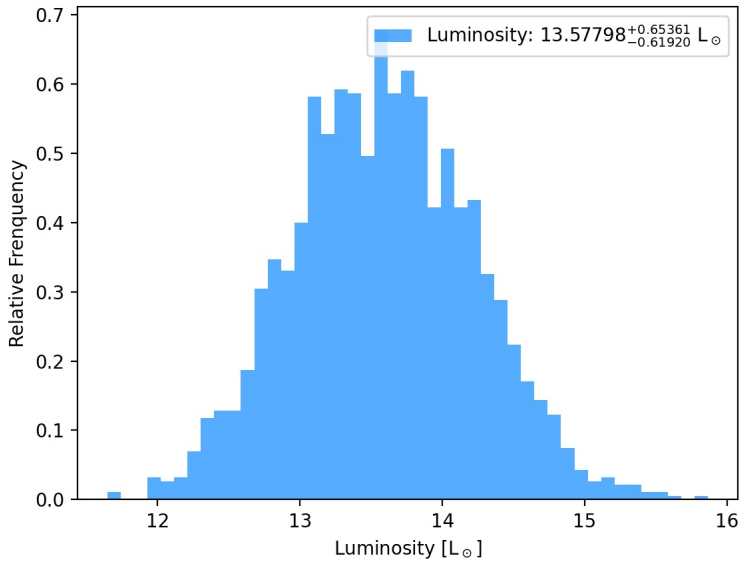

Figure 4-8: v2fit luminosity modeling for HD37601.

Kīauhōkū results for the mass and age of HD37601 are shown in Table 4-3. The standard deviation for the ages is 0.43 — a relatively large spread, with over one Gyr between the lowest value (1.64 Gyr from MIST) and the highest (2.65 Gyr from GARSTEC). HD37601 has the highest mass standard deviation out of all the stars, at 0.10, but not significantly higher — both HD45410 (Table 4-5) and HD200964 (Table 4-7) have mass standard deviations above 0.09.

	yrec	**mist**	**dartmouth**	**garstec**	**mean**	**Std dev**	**Mass offset**
initial_ mass	1.612287	1.774953	1.702919	1.544015	1.658544	0.101286	0.230938
initial_ met	0.140000	0.140000	0.140000	0.139997	0.139999	0.000002	0.000003
eep	564.056913	487.465326	556.942138	568.635196	544.274893	38.177387	81.169870
mass	1.612287	1.774009	1.702919	1.542868	1.658021	0.101359	0.231141

teff	4958.999730	4958.999705	4958.999706	4957.731543	4958.682671	0.634085	1.268187
lum	13.577000	13.576999	13.577001	13.576998	13.576999	0.000001	0.000003
met	0.140000	0.140000	0.140000	0.139997	0.139999	0.000002	0.000003
logg	3.250398	3.290642	3.271481	3.228893	3.260353	0.026646	0.061749
age	2.346093	1.644040	2.002927	2.650069	2.160782	0.434236	1.006028

Table 4-3: Mass and age modeling results for HD37601 from Kīauhōkū

A summary of the measured values and errors for the characteristics of HD37601 is given in Table 4-4. Again, luminosity has the highest error due to propagation. None of the errors is unreasonably large.

	Value	**Upper error**	**Lower error**	**Mean error**	**Percent error**
Angular Diameter (mas)	0.7843	0.020	0.018	±0.019	±2.4%
Radius ($R_\odot$)	4.99	0.17	0.16	±0.17	±3.3%
Effective temperature (K)	4959	58	60	±59	±1.2%
Luminosity ($L_\odot$)	13.58	0.65	0.62	±0.64	±4.7%
	Value	**Std Dev**			
Mass ($M_\odot$)	1.66	0.10	-	-	-
Age (Gyr)	2.16	0.43	-	-	-

Table 4-4: Summary of measured values for HD37601

4.3 HD45410

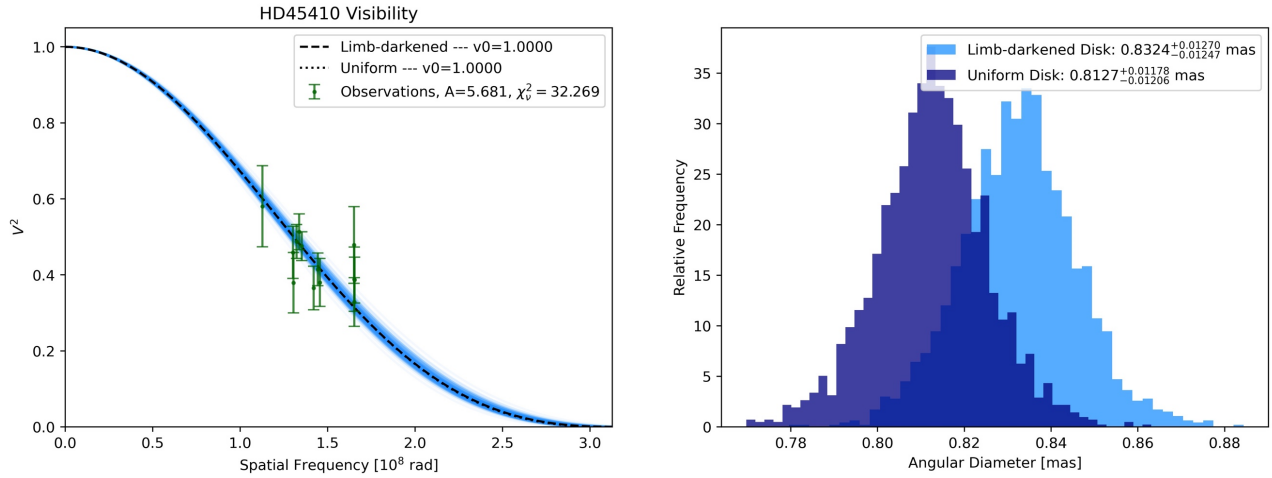

Figure 4-9: v2fit Angular diameter fitting for HD45410

During the fitting process for HD45410 (Figure 4-9), a night of data from 2008 turned out to be unusable and had to be eliminated. On a different night, a target-star observation had to be cut. There still proved to be plenty of good observations for the fitting process. Despite a high chi-square statistic of 32.269, the LDD comes out as 0.8324 ±1.5% mas, with a reasonable error.

The radius is 4.99 ±3.0% solar masses (Figure 4-10), the effective temperature is 4988 ±0.76% K (Figure 4-11), and the luminosity is 13.87 ±0.76% solar luminosities (Figure 4-12). The luminosity error is higher than 5%, but only by an extra 0.2%, making the measurement still reasonably accurate. HD45410 is the most luminous star in the sample, likely because it is the second-hottest star after HD22713 while having a much larger radius than HD22713.

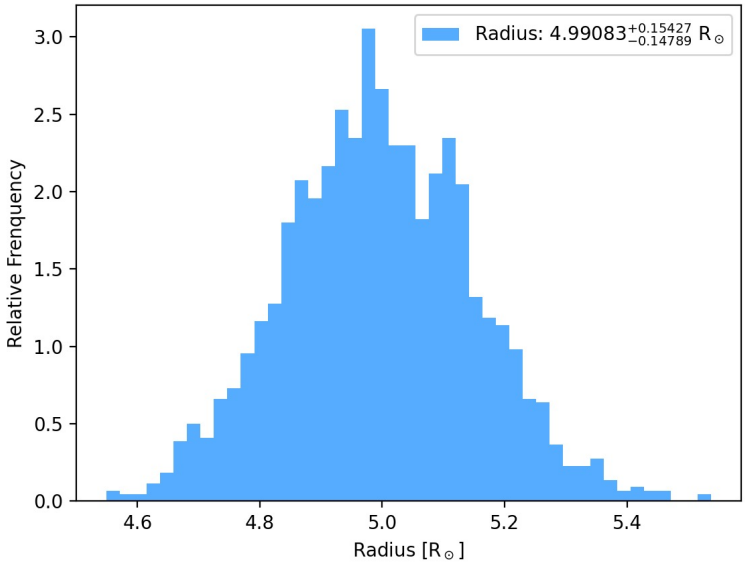

Figure 4-10: v2fit radius modeling for HD45410.

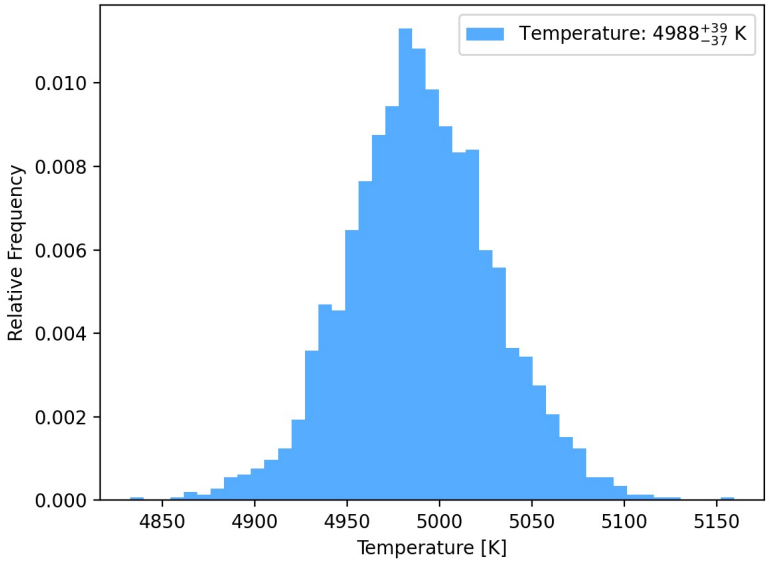

Figure 4-11: v2fit effective temperature modeling for HD45410.

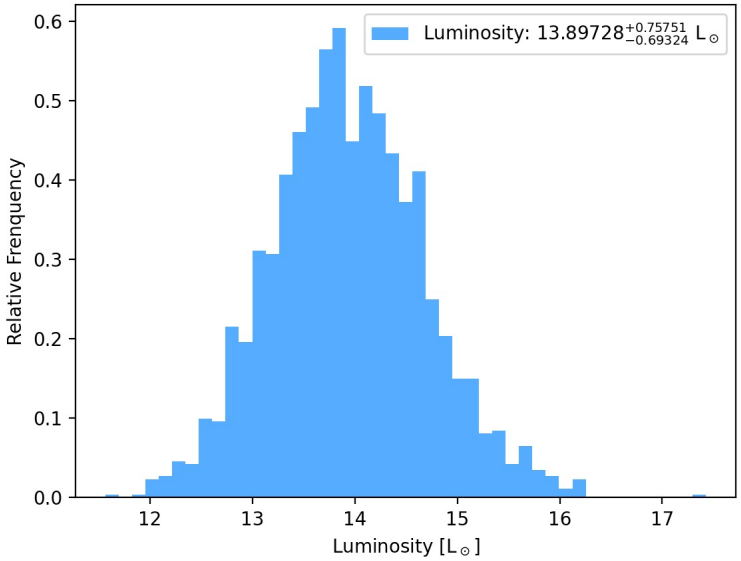

Figure 4-12: v2fit luminosity modeling for HD45410.

The Kīauhōkū output for the mass and age of HD45410 is shown in Table 4-5. The standard deviations for the mass and age are not especially large compared to the other stars in the sample. Nonetheless, the age estimates have a range of more than 1 Gyr, with MIST predicting an age of 1.72 Gyr at the low end and GARSTEC predicting an age of 2.90 Gyr at the high end.

	yrec	**mist**	**dartmouth**	**garstec**	**mean**	**Std dev**	**Mass offset**
initial_ mass	1.571262	1.701740	1.638844	1.484523	1.599092	9.312622e-02	2.172172e-01
initial_ met	0.010000	0.010000	0.010000	0.010000	0.010000	5.126394e-08	1.184856e-07
eep	563.995619	489.916283	560.162250	570.112829	546.046745	3.764401e+01	8.019655e+01
mass	1.571262	1.700809	1.638844	1.483330	1.598561	9.327514e-02	2.174786e-01

teff	4988.000235	4988.000499	4987.999845	4988.000069	4988.000162	2.760958e-04	6.549096e-04
lum	13.867001	13.867000	13.867000	13.867000	13.867000	4.757096e-07	1.063536e-06
met	0.010000	0.010000	0.010000	0.010000	0.010000	5.126394e-08	1.184856e-07
logg	3.238703	3.273218	3.256275	3.212453	3.245162	2.596285e-02	6.076468e-02
age	2.419583	1.721947	2.144048	2.899655	2.296308	4.940642e-01	1.177708e+00

Table 4-5: Mass and age modeling results for HD45410 from Kīauhōkū.

Table 4-6 summarizes the measured values and errors for the characteristics of HD45410. Most of the errors appear reasonable, with the luminosity error being the largest due to propagation from other stellar quantities.

	Value	**Upper error**	**Lower error**	**Mean error**	**Percent error**
Angular Diameter (mas)	0.8324	0.013	0.012	± 0.013	±1.5%
Radius ($R_\odot$)	4.99	0.15	0.15	±0.15	±3.0%
Effective temperature (K)	4988	39	37	±38	±0.76%
Luminosity ($L_\odot$)	13.87	0.76	0.69	±0.73	±5.2%
	Value	**Std Dev**			
Mass ($M_\odot$)	1.60	0.093	-	-	-
Age (Gyr)	2.30	0.49	-	-	-

Table 4-6: Summary of measured values for HD45410

4.4 HD200964

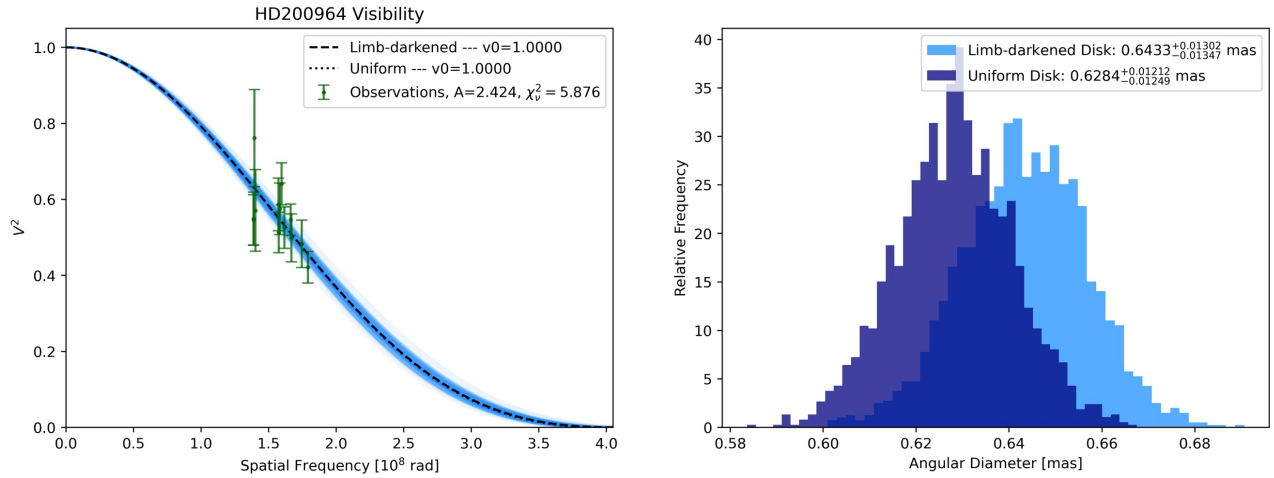

Figure 4-13: Angular diameter fitting for HD200964.

The mean fits for HD200964 have some large error bars and outliers (Figure 4-13). Leaving out a night of data from October 2, 2013 got rid of the outliers, but it was not clear whether these data could justifiably be left out. They remain in the sample for the final calculation, and do not cause egregiously large errors on any parameters in the end.

The chi-square statistic for the fit is 5.876, and the LDD calculation comes out as 0.6433 ±2.1% mas. Given that HD200964 is the most distant star in the sample, it makes sense that its angular diameter is the smallest. However, its estimated radius is the largest in the sample at 5.00 ±4.4% solar radii (Figure 4-14). Its effective temperature is estimated at 4963 ±1.0% Kelvin (Figure 4-15), and its luminosity is 13.67 ±7.9% (Figure 4-16).

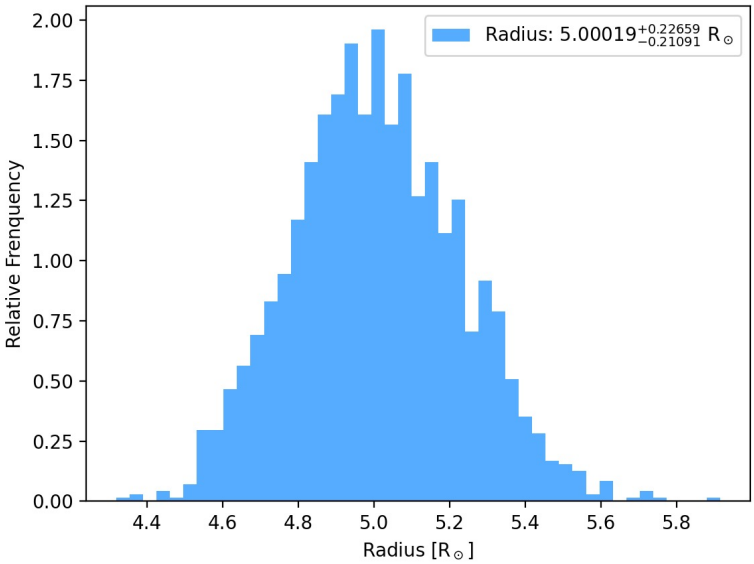

Figure 4-14: v2fit radius modeling for HD200964.

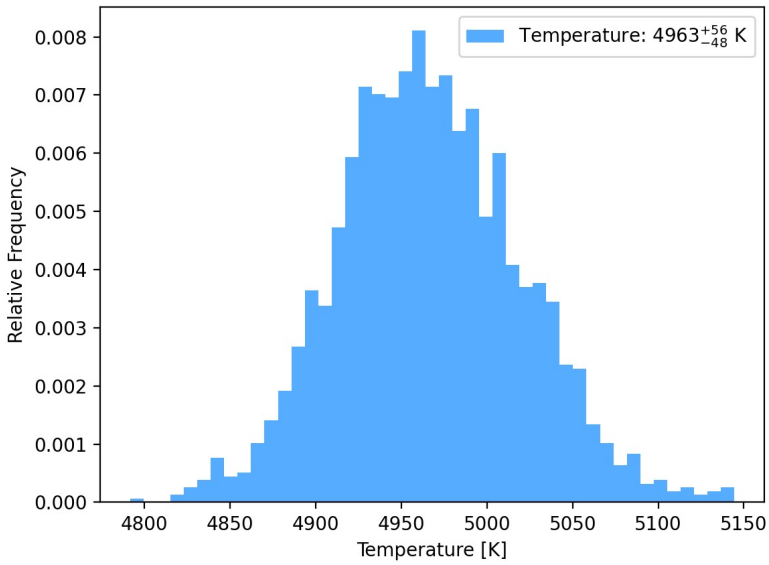

Figure 4-15: v2fit effective temperature modeling for HD200964.

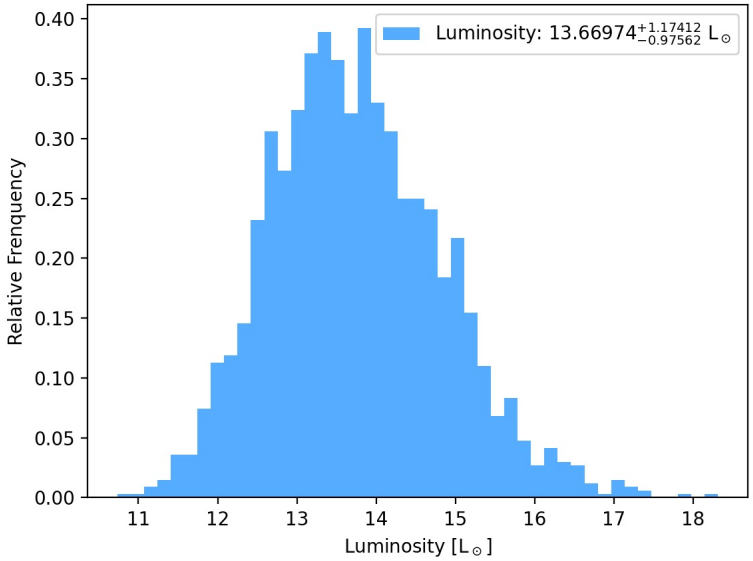

Figure 4-16: v2fit luminosity modeling for HD200964.

The mass standard deviation calculated for HD200964 by Kīauhōkū is 0.096 (Table 4-7), which is a relatively large spread but no worse than most other stars in the sample. The age has an unusual amount of spread, with nearly 2 Gyr between the lowest (from MIST) and the highest (from GARSTEC) estimates.

	yrec	**mist**	**dartmouth**	**garstec**	**mean**	**Std dev**	**Mass offset**
initial_ mass	1.405827	1.524382	1.482494	1.307723	1.430106	9.521813e-02	2.166586e-01
initial_ met	-0.080000	-0.080000	-0.079999	-0.080000	-0.080000	3.256076e-07	7.259130e-07
eep	563.449517	494.101428	567.889512	571.946371	549.346707	3.699329e+01	7.784494e+01
mass	1.405827	1.523455	1.482494	1.304823	1.429150	9.615993e-02	2.186319e-01

teff	4963.000283	4962.999598	4963.011292	4963.002707	4963.003470	5.382447e-03	1.169373e-02
lum	13.669700	13.669701	13.669709	13.669701	13.669703	4.292727e-06	9.107858e-06
met	-0.080000	-0.080000	-0.079999	-0.080000	-0.080000	3.256076e-07	7.259130e-07
logg	3.186874	3.222474	3.209451	3.155932	3.193683	2.914927e-02	6.654178e-02
age	3.379293	2.344498	2.853199	4.330271	3.226815	8.483196e-01	1.985774e+00

Table 4-7: Mass and age modeling results for HD200964 from Kīauhōkū.

Table 4-8 summarizes the measured values and errors for the characteristics of HD200964. The radius and luminosity errors are the highest in the sample, likely due to error propagation from the distance measurement on which both these parameters rely. The distance error for HD200964 is higher than the others because it is the furthest target star from Earth.

	Value	**Upper error**	**Lower error**	**Mean error**	**Percent error**
Angular Diameter (mas)	0.6433	0.013	0.013	±0.013	±2.1%
Radius ($R_\odot$)	5.00	0.23	0.21	±0.22	±4.4%
Effective temperature (K)	4963	56	48	±52	±1.0%
Luminosity ($L_\odot$)	13.67	1.17	0.98	±1.1	±7.9%
	Value	**Std Dev**			

Mass ($M_\odot$)	1.43	0.096	-	-	-
Age (Gyr)	3.23	0.85	-	-	-

Table 4-8: Summary of measured values for HD200964

4.5 HD210702

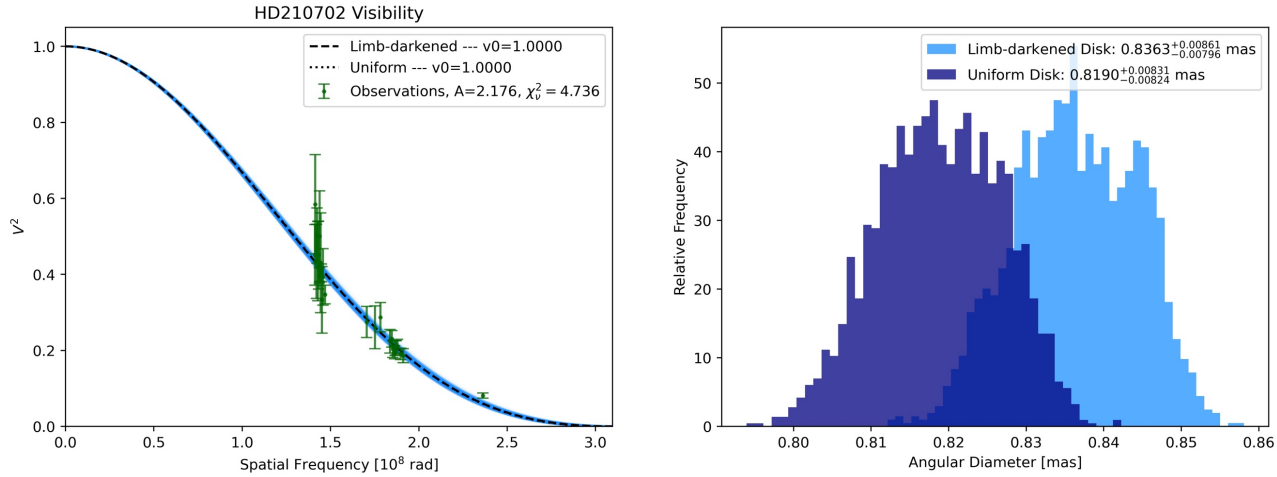

Figure 4-17: Angular diameter fitting for HD210702.

When the median power spectra were used in the fit for HD210702 (Figure 4-17), the resulting graph had enormous error bars on the data points. However, the mean power spectra produces more reasonable results. The chi-square statistic for the fit is 4.736, and the resulting limb-darkened disk measures in at 0.8363 ±1.0% mas.

HD210702 is the coolest star in the sample, with an effective temperature of 4919 ±0.51% K (Figure 4-19). Its radius is estimated as 4.94 ±2.3% (Figure 4-18), and its luminosity is 12.88 ±4.3% (Figure 4-20). Its low temperature makes it less luminous than HD37601, HD45410, and HD200964 despite having a comparable radius.

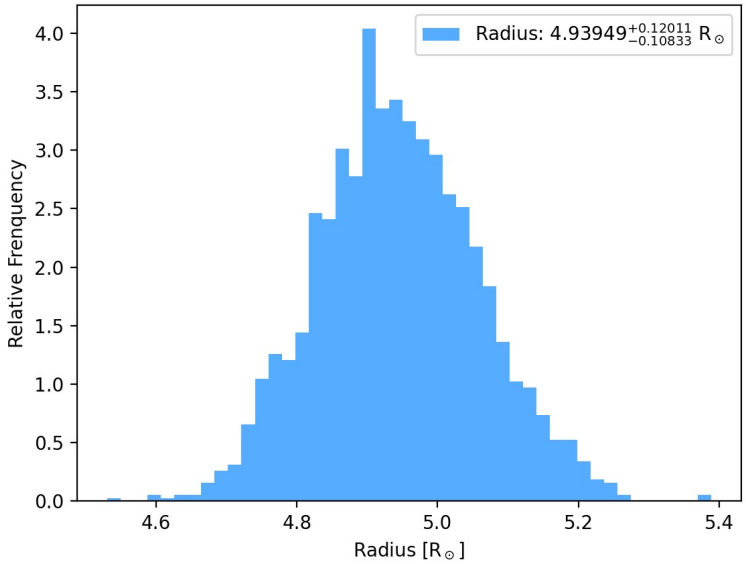

Figure 4-18: v2fit radius modeling for HD210702.

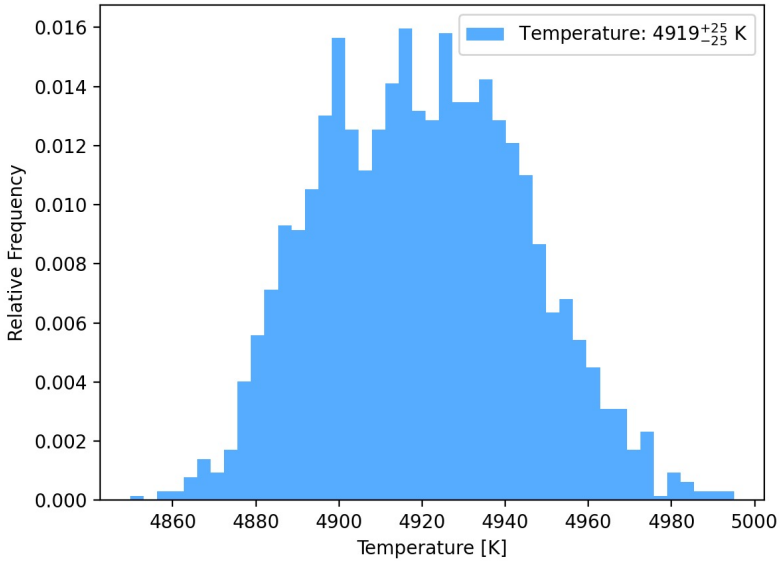

Figure 4-19: v2fit effective temperature modeling for HD210702.

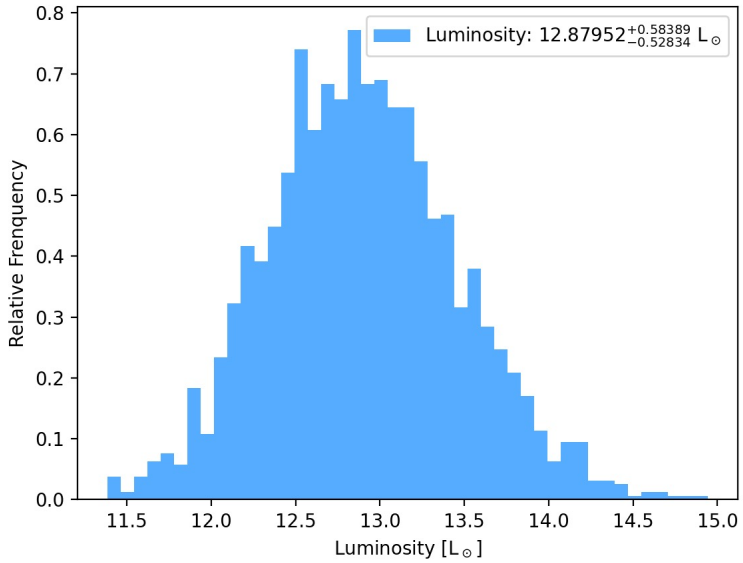

Figure 4-20: v2fit luminosity modeling for HD210702.

In Kīauhōkū, the HD210702 age calculations have a wide spread, with a standard deviation of 1.55. The biggest outlier is the MIST model, which predicts the age of HD210702 as 4.05 Gyr — almost 2 Gyr lower than the next lowest estimate, 6.03 Gyr as predicted by YREC.

Despite the fact that HD210702 is estimated to be larger and more luminous than HD22713, it has the lowest modeled mass of all the stars in the sample, estimated at 1.17 solar masses. Its current mass also deviates the most from its initial mass out of all the stars. This is because the YREC, Dartmouth, and GARSTEC models predict HD210702 to be the oldest star in the sample — between 6.03 and 7.66 Gyr — which gives it more time to lose mass due to winds and other processes that take place in giant stars. However, MIST predicts that HD210702 only has an age of 4.05 Gyr, and therefore does not predict a large difference between the initial and current mass of HD210702.

	yrec	mist	dart-mouth	garstec	mean	Std dev	Mass offset
initial_ mass	1.291354	1.297520	1.328375	1.264866	1.295529	2.607963e-02	6.350846e-02
initial_ met	0.03	0.03	0.03	0.03	0.03	1.830367e-07	4.109293e-07
eep	541.815016	475.700880	539.642171	545.029279	525.546836	3.330424e+01	6.932840e+01
mass	1.179473	1.286716	1.131549	1.093526	1.172816	8.368092e-02	1.931902e-01
teff	4919.002311	4918.998018	4918.999968	4919.000349	4919.000161	1.759540e-03	4.293116e-03
lum	12.879000	12.879000	12.879000	12.879001	12.879000	5.456222e-07	1.317559e-06
met	-0.160000	-0.160000	-0.160000	-0.160000	-0.160000	7.374355e-08	1.678946e-07
logg	3.134495	3.160612	3.130336	3.096018	3.130365	2.653097e-02	6.459432e-02
age	6.031392	4.045078	6.820077	7.661736	6.139571	1.546898e+00	3.616658e+00

Table 4-9: Mass and age modeling results for HD210702 from Kīauhōkū.

.

Table 4-10 provides measurements and errors for the parameters of HD210702. All the errors for the parameters calculated by v2fit are within a reasonable 5%.

	Value	**Upper error**	**Lower error**	**Mean error**	**Percent error**
Angular Diameter (mas)	0.8363	0.0086	0.0080	±0.0083	±1.0%
Radius ($R_\odot$)	4.94	0.12	0.11	±0.11	±2.3%

Effective temperature (K)	4919	25	25	±25	±0.51%
Luminosity ($L_\odot$)	12.88	0.58	0.53	±0.56	±4.3%
	Value	**Std Dev**	-	-	-
Mass ($M_\odot$)	1.17	0.084	-	-	-
Age (Gyr)	6.14	1.55	-	-	-

Table 4-10: Summary of measured values for HD210702

5 DISCUSSION

This section begins by comparing two of the measured angular diameters to previously-measured angular diameters of the same stars to reflect on the accuracy of these measurements (previous interferometric angular diameter measurements were not available for all target stars). The stellar characteristics derived from the interferometric observations of the five target stars are then compared to the values recorded in the literature from photometric and spectroscopic sources. These differences are statistically analyzed and possibilities are presented for the cause of the discrepancies between interferometry-derived and photometry-derived values.

5.1 Angular Diameter Comparisons

Comparing interferometry measurements comes with the caveat that angular diameters can be measured using different instruments. White et al. (2018) suggests that different CHARA beam combiners produce markedly divergent results. One of the stars it deals with is HD45410, noting a previous CLASSIC beam combiner measurement of 0.970 ± 0.035 mas taken in 2009 and a PAVO beam combiner measurement of 0.853 ± 0.013 mas. However, the angular diameter of HD45410 in this thesis was measured as 0.8324±0.013, closer to the PAVO measurement cited in White et al. (2018) and defying the paper's observation that CLASSIC angular diameters tend to be larger than PAVO measurements. White et al. (2018) theorizes that the discrepancy it observes between CLASSIC and PAVO might arise due to targets being under-resolved. Given that the CLASSIC measurement for HD45410 in this thesis uses data from between 2013 and 2017, it stands to reason that recent improvements to the CLASSIC instrument have given it performance comparable to that of PAVO.

Von Braun et al. (2014) provides an angular diameter of 0.886 ± 0.006 mas for HD210702, taken with CHARA's CLASSIC instrument. This is around 6% larger than the value of 0.8363 mas measured here. The measurement for HD210702 in this thesis uses some of the same CHARA observations as von Braun et al. (2014), but also includes some data from 2019. It is possible that improved performance of the CLASSIC instrument resulted in this difference.

The angular diameters calculated for this thesis generally seem robust. The following sections compare the other stellar characteristics calculated from these angular diameters to stellar characteristics from photometry and spectroscopy observations to see how they match up.

5.2 Literature Sources for Stellar Characteristics

Table 5-1 shows the short citation for each paper that provides photometry or spectroscopy-based measurements for the stars in this sample, along with which stars each paper includes and which stellar characteristics they measure. The stars are listed by the first two digits of their HD catalog number — 22 stands for HD22713, 37 stands for HD37601, 45 stands for HD45410, 20 stands for HD200964, and 21 stands for HD210702. Radius is abbreviated as R, effective temperature as T, luminosity as L, mass as M, and age as A.

Literature reference short citation	**Included stars (first two digits of HD number)**	**Quantities measured**
2022yCat.1355....0G	22, 37, 20, 21	R, T (not for 21), L, M, A
2022A&A...657A...7K	22, 37, 45, 20, 21	R, M
2021A&A...653A..98M	22	R, T, M
2020yCat.1350....0G	22	T
2020MNRAS.496.5423M	20	T, L, M
2020ApJS..247...11R	37, 45, 20, 21	T, L, M
2020ApJ...898..119R	22	T
2020ApJ...890...23L	45, 20, 21	L, M

2019ApJS..241...12S	22	R, T, L
2019AJ....158..138S	22, 37, 20, 21	R, T
2019AJ....157..149L	45, 20, 21	R, T, M
2019A&A...628A..94A	22, 37	T, M
2019A&A...623A..72K	22, 37, 45, 20, 21	R, M
2018ApJ...867..105T	22	T
2018ApJ...860..109G	37, 45, 20, 21	R, T, M, A
2018AJ....156..102S	22, 45, 20, 21	R, M
2018A&A...616A...1G	22, 37, 45, 20, 21	R, T, L
2018A&A...615A..31D	45, 20	R, T, L, M, A
2017MNRAS.471..770M	22, 37, 45, 20, 21	R, T, L
2017AJ....154..259S	22	T
2017AJ....154..115H	22, 37, 45, 20, 21	L
2017AJ....153..136S	20	R, M
2017AJ....153...21L	22	L, M, A
2016ApJS..225...32B	37, 45, 20, 21	R, T (not for 37), L, M, A
2016AJ....151...59C	37, 20, 21	T, L
2016A&A...591A.118S	22	T
2016A&A...585A..73N	20	R, T, L, M, A
2016A&A...585A...5B	45, 20, 21	R, T, L, M, A
2015A&A...576A..94S	45	R, T, M, A
2015A&A...575A..18B	45, 20, 21	R, T, L, M, A
2015A&A...574A..50J	20, 21	R, T, L, M, A
2015A&A...573A..67P	22	T
2014PASP..126..469P	22	T
2014MNRAS.444.3517M	22	R, T, L, M, A
2013A&A...554A..84M	22, 20, 21	R, T, L, M, A
2012MNRAS.427..343M	37, 20, 21	T, L
2012AstL...38..331A	22, 37, 45, 20, 21	L
2008AJ....135..209M	22, 37, 45, 20, 21	R, T, L
2007ApJS..168..297T	22	R, T, M
2006ApJ...638.1004A	22	T
2005ApJS..159..141V	22	T, M, A
2003AJ....125..359W	22	T
2001A&A...377..911F	22	T, M, A
2001A&A...367..521P	45	R
1999A&A...352..555A	22, 37, 45, 20, 21	R, T (not for 22), L, M, A

Table 5-1: Photometry-based literature sources with the stars included and quantities measured.

For the rest of this chapter, values measured for this research project will be referred to as "interferometry values" and literature values derived from photometry or spectroscopy will be referred to as "photometry values."

5.3 Radius

Interferometry measures the stellar radius based on angular diameter, while photometric methods require a series of models to derive the radius of a star. This makes interferometry the most direct method of stellar radius measurement.

However, interferometry can only be used to measure the radii of bright, nearby stars. The radii for more distant stars can only be determined through photometry. This makes the radius comparison with photometry values especially important — testing photometry-derived radii against interferometry-derived radii will show how accurately photometric technology can measure retired A star radii.

5.3.1 Radius Literature Comparison

The dot plot in Figure 5-1 shows a comparison between the interferometry and photometry values for the radius of each star. Most photometry values (shown in blue) did not report errors for the stellar parameters, but those that did report errors have been plotted with error bars. The orange interferometry values all have error bars.

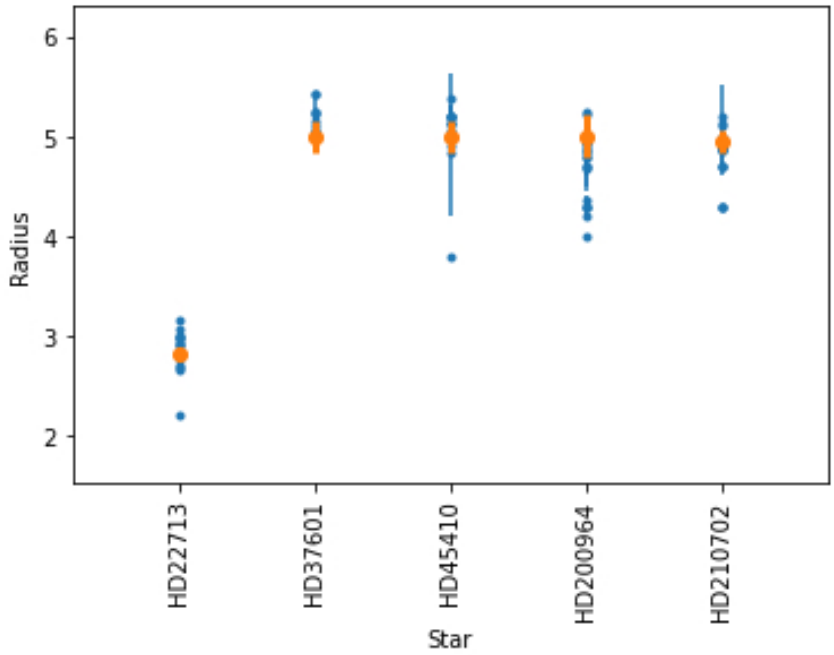

Figure 5-1: Comparing the measured values for each star's radius in solar radii to the values given in the literature. The smaller blue points represent literature photometry values and the larger orange points represent measured interferometry values.

The interferometry values for the stars' radii are within the range of the photometry values, but most are toward one end or the other of the range. The interferometry measurements for HD22713, HD37601, and HD45410 are on the lower end of the photometry values, while the measurement for HD200964 is toward the higher end of the range and the measurement for HD210702 is close to the middle.

Two especially interesting sets of radius values come from Kervella et al. (2019) and Kervella et al. (2022). These papers aim to calculate the proper motion anomaly of various stars to detect exoplanets around them, a procedure that requires knowledge of a stellar radius. Both publications find stellar radii using photometric color as an input, but instead of using the regular types of isochrone models to find stellar radii, the color is run through an equation for a color-angular diameter relationship. This relation, established in Kervella et al. (2004), was created by

taking interferometrically-measured angular diameters and photometrically-measured effective temperatures for the same stars and working out an equation to relate the two. The Kervella et al. (2019) and Kervella et al. (2022) values for HD210702 represent noticeable outliers for this star, with all other photometry values and the interferometry value being larger. For HD200964 and HD37601, the Kervella et al. (2019) and Kervella et al. (2022) values are the largest in the photometry sample. For HD22713, the values are on the lower end of the range, but are not the lowest in the photometry sample. For HD45410, the values are very close to the photometry median.

The low outlier for HD45410 comes from Pasinetti-Fracassini et al. (2001), which details the Catalogue of Stellar Diameters (CADARS). The data in this catalog come from a variety of sources, but the radius measurement for HD45410 was sourced from a photometric determination by Wesselink (1969). This paper used an H-R diagram to find stellar radii — the more complex methods of modelling radii from photometry did not exist back in 1969. It is likely that the underestimated radius for HD45410 in this source is due to an outdated and imprecise methodology.

5.3.2 Radius Sigma Offset Analysis

A sigma offset is a measurement of the deviation between one value and another. In this case, taking the sigma offset is a way of measuring the deviation between the photometry median and interferometry values of each star parameter. The photometry median, rather than the mean, was chosen to avoid outliers affecting the result.

The sigma offset from the literature median for each parameter was calculated using the formula:

$$\sigma = \frac{v_m - v_l}{e_m}$$

In this equation, σ is the sigma offset, v_m is the interferometry-derived value for the star parameter calculated in Chapter 4, v_l is the median photometry-derived value for the same star parameter, and e_m is the error for the interferometry-derived parameter. Errors for the interferometry-derived radius, luminosity, and temperature were calculated by the v2fit code.

Radius (R⊙)	Interferometry value	Photometry median	Interferometry error	Sigma Offset
HD22713	2.83	2.92	0.04	-2.5
HD37601	4.99	5.18	0.17	-1.2
HD45410	4.99	5.12	0.15	-0.9
HD200964	5.00	4.78	0.22	1.0
HD210702	4.94	4.89	0.11	0.4

Table 5-2: Sigma offsets between interferometry and photometry radius values, and the values used to calculate the sigma offset.

The interferometry-derived radius for HD22713 has the greatest sigma offset of all the star radii — 2.5 sigma offsets below the median photometry-derived value (Table 5-2). The closest-matching radius is HD210702, with an interferometry value only 0.4 sigma offsets above the photometry median.

The sigma offsets for the interferometry radius values do not match up with the offsets for the Kervella et al. (2019) and Kervella et al. (2022) radius values, despite these two papers using an interferometry-derived relationship to process photometry data. Where the papers drastically underestimate the radius of HD210702, the measured interferometry value for the same star is close to the photometry median. The radii for HD200964 and HD37601 are both overestimated by Kervella et al. relative to the photometry median, while the interferometry values overestimate HD200964 and underestimate HD37601. HD22713 is underestimated by

both Kervella et al. and the interferometry values, but the Kervella et al. values fall further below the photometry median. The interferometry radius for HD45410 is underestimated compared to the literature median, but the Kervella et al. values are very close to the median. This suggests that deriving stellar radii from a color-angular diameter relationship is not equivalent to measuring radius from the angular diameter directly.

Yee et al. (2017) is a paper that tests the spectral modelling tool "Empirical SpecMatch" (SpecMatch-Emp) by comparing its results to directly measured values from other literature. In some cases, the spectroscopy-derived SpecMatch-Emp radius was compared to to interferometry-derived radii. Yee et al. (2017) found that overall, the SpecMatch-Emp model results deviated by around 15% from the library data, though not all of the library radii were derived from interferometry due to the scarcity of interferometry measurements for many stars. By contrast, the percent differences between the interferometry value and photometry median for all the stars in this thesis target sample are under 5%, suggesting that, on average, photometry radii are closer to the interferometry radii than Yee et al. (2017) might posit.

The fact that the interferometry-derived radii are all within the range of the photometry-derived radii is a good sign that they are at least comparable methods of radius measurement. This is promising for radius measurements of more distant stars that cannot be measured with interferometry.

5.4 Effective Temperature

Effective temperature is closely related to the color of a star, which is directly measured with photometry. Finding the effective temperature from interferometry requires outside data about the bolometric flux of a star. Photometry can be considered a more direct measurement of stellar temperature than interferometry.

5.4.1 Effective Temperature Literature Comparison

Figure 5-2 shows a comparison between the interferometry-derived effective temperature and photometry-derived values for effective temperature.

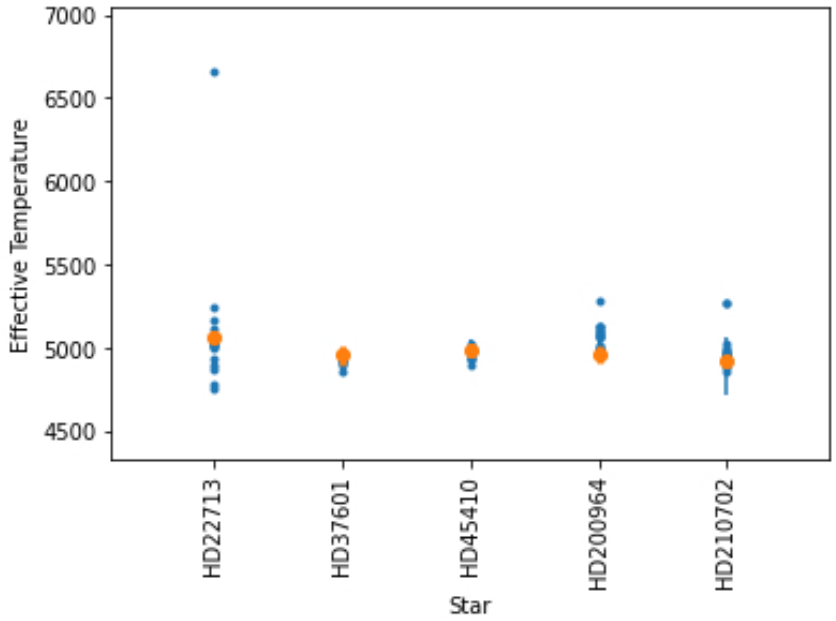

Figure 5-2: Comparing the measured values for each star's effective temperature in Kelvin to the values given in the literature. The smaller blue points represent literature photometry values and the larger orange points represent measured interferometry values.

The interferometry-derived effective temperature data point for HD22713 sits right around the median. The high photometry temperature outlier for this star comes from Ander et al. (2019), a paper that uses Gaia parallaxes and optical photometry from various sources to get stellar parameters from modelling. The project used the catalog of data to map the shape of the Milky Way, creating a clear picture of the galaxy's bar that suggests the overall data distribution was not suspect. The paper claims that brighter stars should have more accurate results, and

HD22713 is bright enough to be visible with the naked eye. It is unclear why the model produced such a large result for this star.

The interferometry data points for HD37601 and HD45410 sit toward the higher end of their ranges, though the photometry data remain closely clustered around the interferometry data. The interferometry temperatures for HD200964 and HD210702 appear on the lower end of the photometry range, and noticeable upper-end outliers exist for both of these stars. The outlier for HD200964 comes from the Gaia Data Release 3 (Gaia Collaboration, 2022), and represents a temperature calculated from Gaia's spectrophotometers. The HD210702 outlier is actually from two papers — McDonald et al. (2012) and Chandler et al. (2016), both of which report the effective temperature as 5264 K. Chandler et al. (2016) follows the same procedure as McDonald et al. (2012), re-reducing the data to confirm the results, and proceeds to map the habitable zones of stars in our solar neighborhood. For all of these outliers, it is unclear why they deviate from the rest of the data, but it must be noted that these outliers are not far from the range of the rest of the values, especially when compared to the spread of values for HD22713.

5.4.2 Effective Temperature Sigma Offset Analysis

Effective Temperature (K)	Interferometry value	Photometry median	Interferometry error	Sigma Offset
HD22713	5061	5042	17	1.1
HD37601	4959	4931	59	0.5
HD45410	4988	4975	38	0.3
HD200964	4963	5062	52	-1.9
HD210702	4919	4954	25	-1.4

Table 5-3: Sigma offsets between interferometry and photometry effective temperature values, and the values used to calculate the sigma offset.

The interferometry-derived effective temperature for HD200964 has the largest deviation from the photometry values, at 1.9 sigma offsets below the photometry median (Table 5-3). For HD45410, the interferometry value is only 0.3 sigma offsets above the photometry median. The negative sigma offsets for effective temperature are more severe, but three out of five stars have positive sigma offsets.

Boyajian et al. (2013) is a paper that derives the effective temperatures of 68 main-sequence stars from interferometry and compares them to spectroscopically-determined effective temperatures from the same stars. The project reports only a 1.7% offset between the temperatures, with the interferometry values trending lower. It is not clear whether this result would extend to evolved stars like the retired A stars in this thesis sample. However, the percentage differences between the interferometry measurements and photometry medians for each retired A star in this thesis are all 1.97% or less. Another paper, Mann et al. (2015), finds "excellent" agreement between temperatures derived from interferometric measurements and temperatures derived from spectra for K and M main-sequence stars. This suggests that interferometry and photometry-derived temperatures may be close for all types of stars.

White et al. (2018) compares interferometry-derived effective temperatures of retired A stars to photometry-derived effective temperatures. The paper noted that, while its angular diameter measurements disagreed by up to 30% with previous angular diameter measurements of the same stars, the effective temperatures derived from its own interferometry measurements matched well with the effective temperatures determined through photometry and spectroscopy. The paper theorizes that the close match is due to the increased resolution of more recent interferometry measurements, which leads to more accurate determination of other stellar characteristics. This is consistent with the relatively small deviations between the interferometry

and photometry-derived effective temperatures here. It appears that advances in interferometer resolution may now allow for accurate measurements of effective temperature using either interferometric or photometric methods.

5.5 Luminosity

Luminosity comes from the effective temperature and radius of a star, but may also be calculated using the bolometric flux and distance to a star. Either of these methods could theoretically be used for finding luminosity from interferometry or photometry data, depending on what other parameters are available. The v2fit code used for this thesis combined interferometry values from CHARA with bolometric flux and distance to find stellar luminosities.

5.5.1 Luminosity Literature Comparison

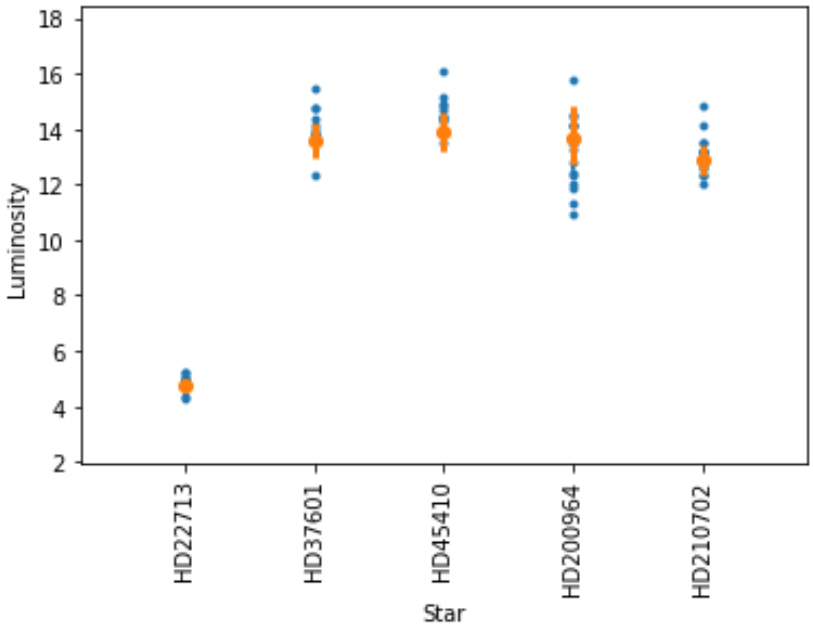

Figure 5-3: Comparing the measured values for each star's luminosity in solar luminosities to the values given in the literature. The smaller blue points represent literature photometry values and the larger orange points represent measured interferometry values.

Figure 5-3 shows a comparison between the interferometry and photometry values for the luminosity of each star. The photometry values cluster very tightly around HD22713, so it is hard to tell how far it deviates from the interferometry value. The luminosity sigma offset analysis in Section 5.5.2 will shed more light on this. The interferometry values for HD37601 and HD45410 appear to be on the lower end of the photometry value range, while the HD200964 interferometry value is on the higher end. HD210702 has a few photometry-derived outliers, but the interferometry value fits nicely into the main cluster of photometry-derived data points.

The highest luminosity values for HD22713, HD45410, HD37601, and HD210702 were all sourced from Anderson and Francis (2012), a catalog of Hipparcos data cross-referenced with data from other sources. The paper notes that its luminosity values did not take interstellar absorption into account, and therefore may be inaccurate for very distant stars or stars close to the galactic equator. The target stars fall into neither of these categories, so it is unclear why these luminosity measurements are so high. A systematic error in the paper's method may be to blame, especially since Anderson and Francis (2012) is also responsible for the second-highest luminosity value for HD200964.

The upper outlier for HD200964 comes from the Gaia Data Release 3 (Gaia Collaboration, 2022), the same publication that provided a large temperature estimate for this star as mentioned in Section 5.4.1. Luminosity is directly related to temperature, so it is no surprise that Gaia Collaboration (2022) also gave a large value for this star's luminosity. The publication gives a radius for HD200964 close to the photometry median radius, so the overestimation of luminosity is likely due almost completely to an overestimation of temperature.

5.5.2 Luminosity Sigma Offset Analysis

Luminosity (L⊙)	Interferometry value	Photometry median	Interferometry error	Sigma Offset
HD22713	4.72	4.95	0.12	-1.9
HD37601	13.58	14.04	0.64	-0.7
HD45410	13.87	14.45	0.73	-0.8
HD200964	13.67	13.49	1.07	0.2
HD210702	12.88	13.06	0.56	-0.3

Table 5-4: Sigma offsets between interferometry and photometry luminosity values, and the values used to calculate the sigma offset.

Interferometry-derived luminosities for all stars except for HD22713 were less than 1.0 sigma offsets away from the photometry values (Table 5-4). The interferometry value for HD22713 has a large sigma offset of 1.9 below the photometry median. This is likely related to the large sigma offset for the radius of HD22713 noted in Section 5.6.1, since stars with a smaller radius are less luminous.

A previously mentioned, it seems likely that radius and temperature can be measured to high precision with interferometry or photometry. Luminosity is a function of both these quantities, so the findings for radius and temperature are likely to hold for luminosity. These three stellar parameters were all calculated using a simple fitting model with v2fit, which keeps assumptions about complex stellar physics to a minimum. The lack of dependence on stellar quantities that are not directly measurable contributes to the ease of determining these values.

5.6 Mass

Finding the mass of a star requires knowing its luminosity and temperature and fitting it to a Herzsprung-Russell diagram to find out which stellar mass it most closely resembles. This means

both interferometry and photometry measurements must go through model-fitting processes to obtain this stellar characteristic.

5.6.1 Mass Literature Comparison

Figure 5-4 shows a comparison between the photometry-derived and interferometry-derived values for the mass of each star.

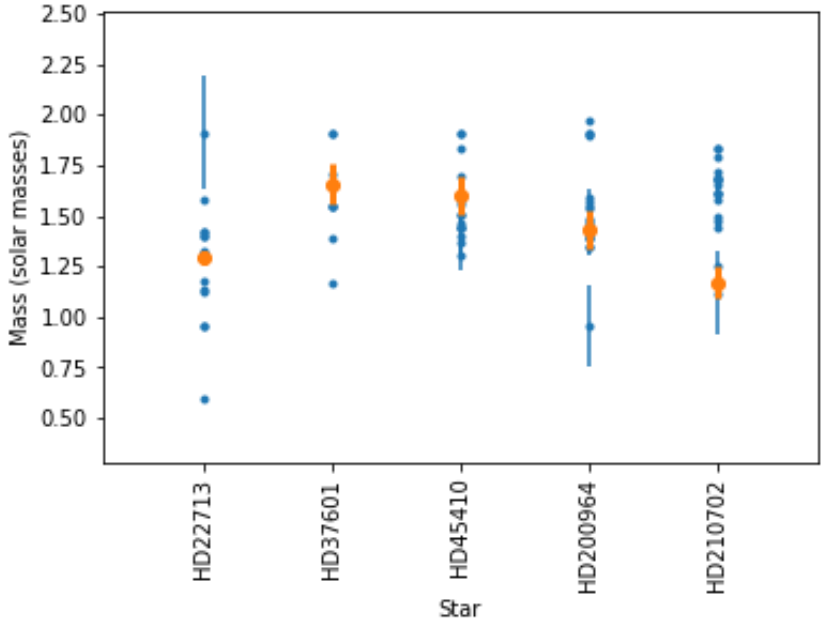

Figure 5-4: Comparing the measured values for each star's mass in solar masses to the values given in the literature. The smaller blue points represent literature photometry values and the larger orange points represent measured interferometry values.

A wide spread of photometry-derived masses exist for each target, but the interferometry data points mostly fit around the middle of the photometry ranges. HD210702 is a notable exception, with the interferometry data point sitting at the very bottom of the photometry range.

Two of the sources for HD22713 report its mass as less than one solar mass, taking it out of the retired A star category. One of these is Feltzing et al. (2001), a paper that aims to explore

the age-metallicity relation in the solar neighborhood. The values from this paper are suspect due to its unusually high age estimate for HD22713, which will be further discussed in Section 5.7.1. Allende Prieto and Lambert (1999) estimates the mass of HD22713 as 0.96 solar masses through a process that involves mapping stars onto an H-R diagram. This paper notes that its overall sample is biased toward main-sequence stars and solar-mass stars, so the fact that HD22713 is a subgiant may account for the inaccurate mass estimate.

A library value from Yee et al. (2017) estimates the mass of HD200964 as 0.96 solar masses, though this value has a relatively large error of ±0.2 solar masses attached. The reason for this mass underestimation is unclear, but the same source provides an unusually high age estimate for this star (see Section 5.7.1), so the values are suspect.

5.6.2 Mass Sigma Offset Analysis

Kīauhōkū did not supply errors for the masses and ages of the target stars, so the mass and age sigma offsets were instead calculated using the standard deviation of the results from the four models. This still provides a quantitative measure of the difference between the interferometry and photometry values for mass and age.

Mass (M⊙)	Interferometry value	Photometry median	Interferometry error	Sigma Offset
HD22713	1.29	1.36	0.03	-2.5
HD37601	1.66	1.55	0.10	1.0
HD45410	1.60	1.49	0.09	1.2
HD200964	1.43	1.47	0.10	-0.4
HD210702	1.17	1.63	0.08	-5.5

Table 5-5: Sigma offsets between interferometry and photometry mass values, and the values used to calculate the sigma offset.

The mass sigma offset for HD210702 is the largest out of all the target stars — 5.5 sigma offsets below the literature median (Table 5-5). HD22713 also has a large sigma offset of -2.5. All other star masses have sigma offsets that are less severe in magnitude.

White et al. (2018) found that masses derived from spectroscopic parameters tended to be larger than those derived from interferometric parameters. However, the paper also notes that mass results may be heavily affected by the specific model used to calculate them. Similarly, Tayar et al. (2022) notes that model-derived parameters like mass and age are heavily affected by the ways various models assume interior stellar physics. This latter paper also used Kīauhōkū and the YREC, GARSTEC, MIST, and Dartmouth stellar evolution models, so its conclusions are especially relevant to this thesis. While Tayar et al. (2022) notes that direct angular diameter measurements from interferometry can help reduce uncertainty in the models, and that much of the deviations between models can be explained with observational uncertainty, it suggests that mass modelling results for the same stars often differ by around 5% (and sometimes more) due to procedural differences.

Tayar et al. (2022) recommends comparing the results from several models to see how much disagreement occurs between models. Accordingly, this thesis uses the mean of the four different models to try and average out model-specific variations, but issues may persist. Mass loss due to star evolution may be especially difficult to account for, which is apparent in the case of HD210702, where three out of four models calculated significant mass loss that led to a severely low mass for this star compared to literature values. The photometry values do not reflect this mass loss, indicating that they may have used models that calculated the stellar physics of this star differently.

It is difficult to make solid conclusions about the difference between interferometry-derived and photometry-derived mass measurements without knowing how much of the difference comes from the models. However, by comparing the four models to each other and to mass estimates from photometry data, it is possible to get an idea of their accuracy.

5.7 Age

Finding the age of a star requires knowledge of its parameters such as mass, temperature, luminosity, and metallicity to compare to an evolutionary model. As with mass measurements, modelling is necessary to find the age of a star no matter whether the directly-measured quantity is a photometric color, a spectrum, or an interferometry-derived angular diameter.

5.7.1 Age Literature Comparison

Figure 5-5 shows a comparison between the photometry and interferometry values for the age of each star.

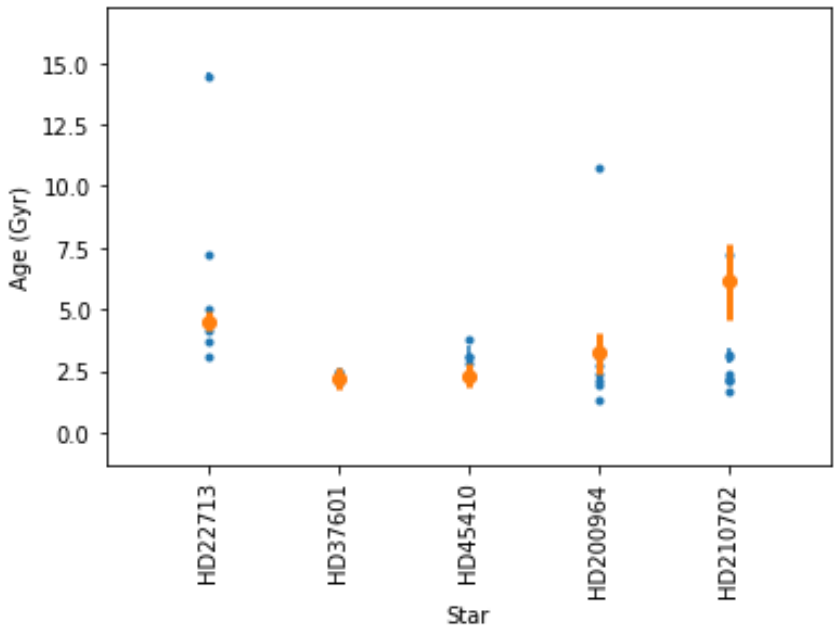

Figure 5-5: Comparing the measured values for each star's age in Gyr to the values given in the literature. The smaller blue points represent literature photometry values and the larger orange points represent measured interferometry values.

The interferometry age for HD22713 sits in the middle of the photometry range, while the HD45410 interferometry value sits at the bottom of the photometry range and the HD200964 interferometry value is on the higher end. The interferometry-derived age for HD210702 is far above that of most photometry values. The photometry data points for HD37601 cluster tightly around the interferometry value, making it difficult to tell where it sits within the photometry range. The sigma analysis for age in Section 5.7.2 will shed light on these situations.

The high outlier for HD22713 is from Feltzing et al. (2001), and estimates HD22713 to be about as old as the universe, which is highly unlikely. This paper also estimates the mass and temperature of HD22713 to be 0.959 solar masses and 4786 Kelvin respectfully — less than most other papers estimate. It lists the metallicity as -0.09, indicating a metal-poor star that might have come from an older generation of star formation. This thesis uses the more recent metallicity value of 0.03 from Luck et al. (2017), which indicates a more metal-rich star that

could have come from a later generation. All this suggests that the high age estimate for HD22713 from Feltzing et al. (2001) might be due to modelling the star using questionable physical parameters as inputs.

The high outlier for HD200964 comes from the library used in Yee et al. (2017). This source also gave a surprisingly low mass estimate for HD200964, as discussed in Section 5.6.1., which suggests that the reasons for the unusual values may be connected. Yee et al. (2017) is also responsible for the only photometric value higher than the interferometry-derived age of HD210702. It is possible the model used to generate these values puts a higher emphasis on mass loss due to age, and produced unusual results for these stars because of this.

5.7.2 Age Sigma Offset Analysis

Age (Gyr)	Interferometry value	Photometry median	Interferometry error	Sigma Offset
HD22713	4.49	4.56	0.39	-0.2
HD37601	2.16	2.49	0.43	-0.8
HD45410	2.30	3.10	0.49	-1.6
HD200964	3.23	2.90	0.85	0.4
HD210702	6.14	2.28	1.55	2.5

Table 5-6: Sigma offsets between interferometry and photometry age values, and the values used to calculate the sigma offset.

The interferometry-derived age for HD210702 is far above that of most photometry ages, which have a median value of 2.28 Gyr compared to the interferometry value of 6.14 Gyr (Table 5-6). The sigma offset is 2.5 above the photometry median. This matches up with the large negative sigma offset for the mass of HD210702 discussed in section 5.6.2 — because the interferometry-derived mass is much lower than the photometry median, it makes sense that the interferometry-derived age is higher to account for the star losing mass as it ages.

None of the other interferometry values has a sigma offset as severe as HD210702, but there is still a range from 0.2 sigma offsets away from the photometry median for HD22713 to 1.6 sigma offsets away from the photometry median for HD45410.

Tayar et al. (2022) reports that age modelling results for subgiant stars often differ by around 20%, and sometimes more. This is apparent in the spread of values for the four models used in this thesis and in the spread of photometry-derived age estimates. As with mass, it is difficult to tell how much of the variation between interferometry-derived and photometry-derived age measurements comes from the input values and how much comes from the differences in models used. However, given the close agreement between interferometry-derived and photometry-derived radius, temperature, and luminosity values, it seems likely that most of the large discrepancies come from the models themselves.

5.8 Sigma Analysis Summary and Trends

The bar graph in Figure 5-6 shows the sigma offsets for all the stellar characteristics to help visualize the severity of the deviations between the photometry and interferometry values for each star.

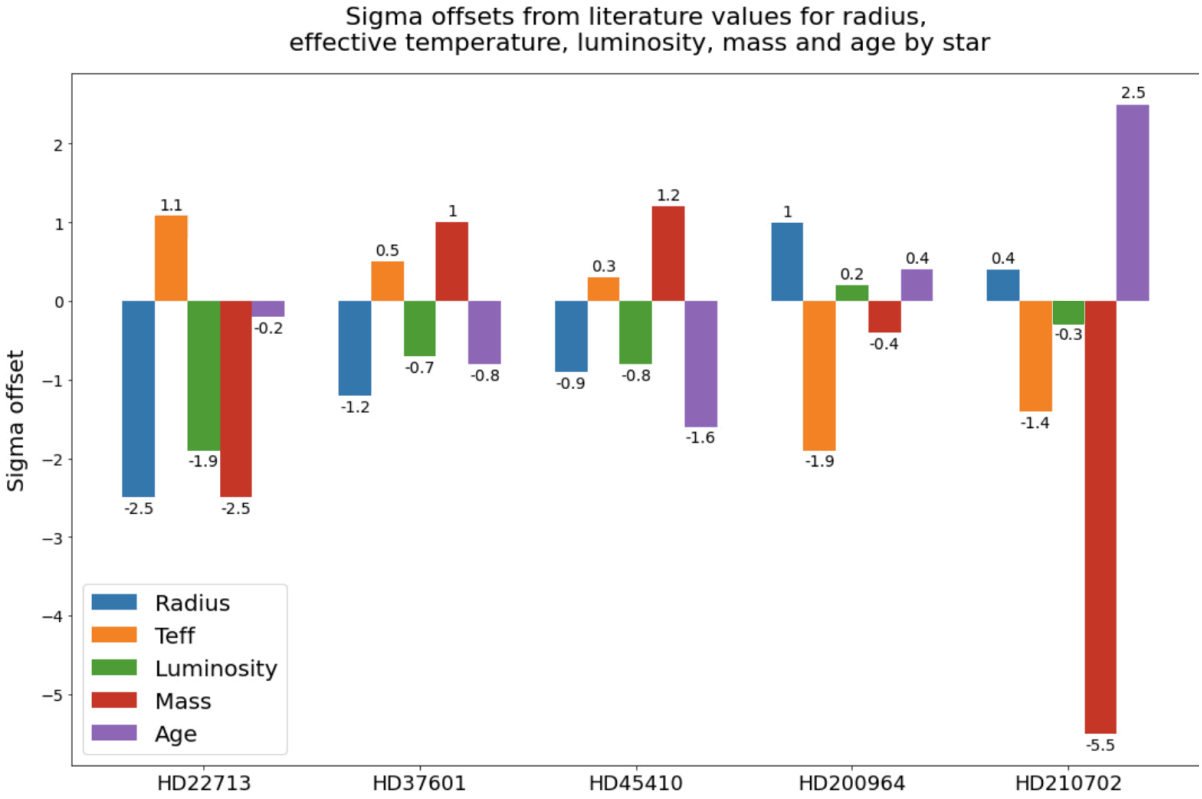

Figure 5-6: Bar graph of the sigma offset between the measured interferometry values and literature photometry median values for the parameters of each star.

Figure 5-6 reveals that the interferometry-derived measurements sometimes have significant deviation from the photometry-derived measurements. Other times, the interferometry-derived and photometry-derived measurements are very close together. There does not appear to be a systematic offset between the values. All of the stars have at least one interferometry value within 0.5 sigma offsets of the photometry median and at least one interferometry value equal to or greater than 1.2 sigma offsets from the photometry median.

Some patterns that emerge are due to mathematical relationships between stellar parameters. For example, interferometry luminosities and radii appear to be underestimated or overestimated in tandem compared to the photometry values. This is likely because a larger radius equates to a larger luminosity, assuming effective temperature holds steady.

The lack of obvious systematic offsets may indicate that discrepancies between interferometry-derived and photometry-derived values are largely to do with observational variances. The relatively close photometry-derived and interferometry-derived quantities for radius, temperature, and luminosity support this conjecture. In the case of mass and age, it is likely that the different models used in various papers produce differing values due to specialized ways of handling stellar physics, on top of effects from observational variance.

5.9 Future Work

Comparisons between stellar parameters derived using different observational methods — especially those calculated by the v2fit code — indicate a promising similarity between interferometry-derived and photometry-derived values. However, this thesis is based only on observations of five retired A stars. A stronger conclusion could be drawn if the procedure was repeated with a larger sample of retired A stars.

The amount of available interferometry data for retired A stars could be increased if existing observations from different CHARA instruments could be combined. Improvements to the CLASSIC instrument have greatly decreased the discrepancies between instruments discussed in White et al. (2018). Therefore, it may be possible to combine data from the CLASSIC and PAVO instruments, and perhaps additional CHARA instruments, to broaden the dataset. Several retired A stars that have been observed with PAVO but not CLASSIC could be added to the sample this way.

In the case of mass and age, deviations between the processes of different models make it difficult to tell how well interferometry and photometry data currently predict these retired A star quantities. Future comparisons between mass and age estimates derived from different

observational techniques would be easier to make if the same models were used to process both types of input. It may be necessary to calculate mass and age in the same publication, rather than using a literature comparison, to ensure a consistent process.

5.10 References

Allende Prieto, C., and D.L. Lambert. “Fundamental parameters of nearby stars from the comparison with evolutionary calculations: masses, radii and effective temperatures.” Astronomy and Astrophysics, v.352 (December 1999).

Ammons, S. Mark, et al. “The N2K Consortium. IV. New Temperatures and Metallicities for More than 100,000 FGK Dwarfs.” The Astrophysical Journal, Volume 638, Issue 2 (February 2006).

Anders, F., et al. “Photo-astrometric distances, extinctions, and astrophysical parameters for Gaia DR2 stars brighter than G = 18.” Astronomy & Astrophysics, Volume 628, id.A94 (August 2019).

Anderson, E., and Ch. Francis. “XHIP: An extended hipparcos compilation.” Astronomy Letters, Volume 38, Issue 5 (May 2012).

Bonfanti, A., et al. “Age consistency between exoplanet hosts and field stars.” Astronomy & Astrophysics, Volume 585, id.A5 (January 2016)

Bonfanti, A., et al. “Revising the ages of planet-hosting stars.” Astronomy & Astrophysics, Volume 575, id.A18 (March 2015).

Bourges, L., et al. “JMMC Stellar Diameters Catalogue - JSDC. Version 2.” VizieR On-line Data Catalog: II/346 (January 2017).

Boyajian, Tabetha S., et al. “Stellar Diameters and Temperatures. III. Main-Sequence A, F, G, and K Stars: Additional High-Precision Measurements and Temperature Relations.” The Astrophysical Journal, Volume 771, Number 1 (June 2013).

Brewer, John M., et al. “Spectral Properties of Cool Stars: Extended Abundance Analysis of 1,617 Planet-search Stars.” The Astrophysical Journal Supplement Series, Volume 225, Issue 2, article id. 32 (August 2016).

Chandler, Colin Orion, et al. “The Catalog of Earth-Like Exoplanet Survey Targets (CELESTA): A Database of Habitable Zones Around Nearby Stars.” The Astronomical Journal, Volume 151, Issue 3, article id. 59 (March 2016).

Deka-Szymankiewicz, B., et al. “The Penn State - Toruń Centre for Astronomy Planet Search stars. IV. Dwarfs and the complete sample.” Astronomy & Astrophysics, Volume 615, id.A31 (July 2018).

Feltzing, S., et al. “The solar neighbourhood age-metallicity relation - Does it exist?” Astronomy and Astrophysics, v.377 (October 2001).

Gaia Collaboration. “VizieR Online Data Catalog: Gaia DR3 Part 1. Main source.” VizieR On-line Data Catalog: I/355. Originally published in: Astron. Astrophys., in prep. (May 2022)

Gaia Collaboration. “VizieR Online Data Catalog: Gaia EDR3 (Gaia Collaboration, 2020).” VizieR On-line Data Catalog: I/350 (November 2020).

Gaia Collaboration, et al. “Gaia Data Release 2. Summary of the contents and survey properties.” Astronomy & Astrophysics, Volume 616, id.A1 (August 2018).

Ghezzi, Luan, et al. “Retired A Stars Revisited: An Updated Giant Planet Occurrence Rate as a Function of Stellar Metallicity and Mass.” The Astrophysical Journal, Volume 860, Issue 2, article id. 109 (June 2018).

Heller, René, et al. “Optimized Trajectories to the Nearest Stars Using Lightweight High-velocity Photon Sails.” The Astronomical Journal, Volume 154, Issue 3, article id. 115 (September 2017).

Jofré, E., et al. “Stellar parameters and chemical abundances of 223 evolved stars with and without planets.” Astronomy & Astrophysics, Volume 574, id.A50 (February 2015).

Kervella, Pierre, et al. “The angular sizes of dwarf stars and subgiants. Surface brightness relations calibrated by interferometry.” Astronomy and Astrophysics, v.426 (October 2004).

Kervella, Pierre, et al. “Stellar and substellar companions of nearby stars from Gaia DR2. Binarity from proper motion anomaly.” Astronomy & Astrophysics, Volume 623, id.A72 (March 2019).

Kervella, Pierre, et al. “Stellar and substellar companions from Gaia EDR3. Proper-motion anomaly and resolved common proper-motion pairs.” Astronomy & Astrophysics, Volume 657, id.A7 (January 2022).

Loyd, R.O. Parke, et al. “Current Population Statistics Do Not Favor Photoevaporation over Core-powered Mass Loss as the Dominant Cause of the Exoplanet Radius Gap.” The Astrophysical Journal, Volume 890, Issue 1, id.23 (February 2020).

Luck, R. Earle. “Abundances in the Local Region II: F, G, and K Dwarfs and Subgiants.” The Astronomical Journal, Volume 153, Issue 1, article id. 21 (January 2017).

Luhn, Jacon K., et al. “Retired A Stars and Their Companions. VIII. 15 New Planetary Signals around Subgiants and Transit Parameters for California Planet Search Planets with Subgiant Hosts.” The Astronomical Journal, Volume 157, Issue 4, article id. 149 (April 2019).

Maldonado, J., et al. “The metallicity signature of evolved stars with planets.” Astronomy & Astrophysics, Volume 554, id.A84 (June 2013).

Malla, S.P., et al. “VizieR Online Data Catalog: 4 planet-hosting stars asteroseismic masses.” VizieR On-line Data Catalog: J/MNRAS/496/5423 (June 2020).

Mann, Andrew W., et al. “How to Constrain Your M Dwarf: Measuring Effective Temperature, Bolometric Luminosity, Mass, and Radius.” The Astrophysical Journal, Volume 804, Number 1 (May 2015).

Marsden, S.C., et al. “A BCool magnetic snapshot survey of solar-type stars.” Monthly Notices of the Royal Astronomical Society, Volume 444, Issue 4 (November 2014).

Massarotti, Alessandro, et al. “Rotational and Radial Velocities for a Sample of 761 HIPPARCOS Giants and the Role of Binarity.” The Astronomical Journal, Volume 135, Issue 1 (January 2008).

McDonald, I., et al. “Fundamental parameters and infrared excesses of Hipparcos stars.” Monthly Notices of the Royal Astronomical Society, Volume 427, Issue 1 (November 2012).

McDonald, I., et al. “Fundamental parameters and infrared excesses of Tycho-Gaia stars.” Monthly Notices of the Royal Astronomical Society, Volume 471, Issue 1 (October 2017).

Montalto, M., et al. “The all-sky PLATO input catalogue.” Astronomy & Astrophysics, Volume 653, id.A98 (September 2021).

Niedzielski, A., et al. “The Penn State - Toruń Centre for Astronomy Planet Search stars.” Astronomy & Astrophysics, Volume 585, id.A73 (January 2016).

Paletou, F., et al. “Inversion of stellar fundamental parameters from ESPaDOnS and Narval high-resolution spectra.” Astronomy & Astrophysics, Volume 573, id.A67 (January 2015).

Pasinetti Fracassini, L.E, et al. “Catalogue of Apparent Diameters and Absolute Radii of Stars (CADARS) - Third edition - Comments and statistics.” Astronomy and Astrophysics, v.367 (February 2001).

Petit, P., et al. “PolarBase: A Database of High-Resolution Spectropolarimetric Stellar Observations.” Publications of the Astronomical Society of the Pacific, Volume 126, Issue 939 (May 2014).

Reiners, Ansgar, and Mathias Zechmeister. “Radial Velocity Photon Limits for the Dwarf Stars of Spectral Classes F-M.” The Astrophysical Journal Supplement Series, Volume 247, Issue 1, id.11 (March 2020).

Rice, Malena, and John M. Brewer. “Stellar Characterization of Keck HIRES Spectra with The Cannon.” The Astrophysical Journal, Volume 898, Issue 2 (August 2020).

Schofield, Mathew, et al. “The Asteroseismic Target List for Solar-like Oscillators Observed in 2 minute Cadence with the Transiting Exoplanet Survey Satellite.” The Astrophysical Journal Supplement Series, Volume 241, Issue 1, article id. 12 (2019).

Soubiran, Caroline, et al. “The PASTEL catalogue: 2016 version.” Astronomy & Astrophysics, Volume 591, id.A118 (June 2016).

Sousa, S.G., et al. “Homogeneous spectroscopic parameters for bright planet host stars from the northern hemisphere . The impact on stellar and planetary mass.” Astronomy & Astrophysics, Volume 576, id.A94 (April 2015).

Stassun, Keivan G., et al. “Accurate Empirical Radii and Masses of Planets and Their Host Stars with Gaia Parallaxes.” The Astronomical Journal, Volume 153, Issue 3, article id. 136 (March 2017).

Stassun, Keivan G., et al. “The TESS Input Catalog and Candidate Target List.” The Astronomical Journal, Volume 156, Issue 3, article id. 102 (September 2018).

Stassun, Keivan G., et al. “The Revised TESS Input Catalog and Candidate Target List.” The Astronomical Journal, Volume 158, Issue 4, article id. 138, (2019).

Stevens, Daniel J., et al. “Empirical Bolometric Fluxes and Angular Diameters of 1.6 Million Tycho-2 Stars and Radii of 350,000 Stars with Gaia DR1 Parallaxes.” The Astronomical Journal, Volume 154, Issue 6, id.259 (December 2017).

Takeda, Genya, et al. “Structure and Evolution of Nearby Stars with Planets. II. Physical Properties of ~1000 Cool Stars from the SPOCS Catalog.” The Astrophysical Journal Supplement Series, Volume 168, Issue 2 (February 2007).

Tayar, Jamie, et al. “A Guide to Realistic Uncertainties on the Fundamental Properties of Solar-type Exoplanet Host Stars.” The Astrophysical Journal, Volume 927, Number 1 (2022).

Tonry, J.L., et al. “The ATLAS All-Sky Stellar Reference Catalog.” The Astrophysical Journal, Volume 867, Issue 2, article id. 105 (November 2018).

Valenti, Jeff A., and Debra A. Fischer. “Spectroscopic Properties of Cool Stars (SPOCS). I. 1040 F, G, and K Dwarfs from Keck, Lick, and AAT Planet Search Programs.” The Astrophysical Journal Supplement Series, Volume 159, Issue 1 (July 2005).

Von Braun, Kaspar, et al. “Stellar diameters and temperatures – V. 11 newly characterized exoplanet host stars.” Monthly Notices of the Royal Astronomical Society, Volume 438, Issue 3 (March 2014).

Wesselink, A.J. “Surface Brightnesses in the *U, B, V* System with Applications of Mυ and Dimensions of Stars.” *Monthly Notices of the Royal Astronomical Society*, Volume 144, Issue 3 (June 1969).

White, T.R., et al. “Interferometric diameters of five evolved intermediate-mass planet-hosting stars measured with PAVO at the CHARA Array.” Monthly Notices of the Royal Astronomical Society, Volume 477, Issue 4 (July 2018).

Wright, Candace O., et al. “The Tycho-2 Spectral Type Catalog.” The Astronomical Journal, Volume 125, Issue 1 (January 2003).

Yee, Samuel W., et al. “Precision Stellar Characterization of FGKM Stars using an Empirical Spectral Library.” The Astrophysical Journal, Volume 836, Issue 1, article id. 77 (February 2017).

6 CONCLUSION

This project set out to discover whether there are significant differences between the stellar parameters of retired A stars derived from photometric data and those derived from interferometry. Interferometric data from the CHARA Array produced the following angular diameters for the five retired A stars in the sample:

- HD22713: 0.7800 ± 0.6%
- HD37601: 0.7843 ± 2.4%
- HD45410: 0.8324 ± 1.5%
- HD200964: 0.6433 ± 2.1%
- HD210702: 0.8363 ± 1.0%

These angular diameters were run through the v2fit code and the Kīauhōkū stellar modelling utility to find values for each star's radius, effective temperature, luminosity, mass, and age. This process requires inputs for the parallax angle, metallicity, bolometric flux, and logarithm of surface gravity for each star.

A statistical analysis shows that the values derived from interferometry are often comparable to the same values derived from photometric or spectroscopic methods, especially in the case of radius, luminosity, and temperature. This opens up possibilities for combining different types of data for future studies. In the specific case of stellar radius, it is promising that the photometry and interferometry values match so well, given that most stars are too far away to measure their angular diameters directly with interferometry.

The existing deviations between interferometric and photometric values are not consistent between stars and have no clear explanation. Some patterns are due to mathematical relationships between parameters. For example, a larger radius equates to a higher luminosity, so stars with an

overestimated radius may have an overestimated luminosity if their effective temperatures are about the same. The lack of non-mathematical trends may be a sign that discrepancies between interferometry-derived and photometry-derived radii, temperatures, and luminosities are not heavily caused by differences between the methods, but by random observational errors. If this is the case, the comparison indicates that modern photometric devices and interferometers have reached a high level of accuracy in measuring these stellar characteristics. In the case of mass and age, more model-specific comparisons are necessary before a guess can be made about the reason for the deviations between photometric and interferometric values.

The lack of available interferometry data for retired A stars is a limitation of this project. If more interferometry-derived data sets were available for more retired A stars, it is possible a more obvious pattern would emerge and reveal a systematic error between photometric and interferometric values. It appears that the CLASSIC instrument at CHARA now has a comparable performance to that of newer instruments like PAVO, presenting the possibility of combining observations made with different instruments to increase the data pool.

This project represents a small step toward answering the crucial question of whether current models accurately predict the characteristics of retired A stars. The results suggest that modern observational instruments have made excellent strides toward accurately measuring retired A star parameters. These more precise measurements will be crucial to future searches for the exoplanets that may be lurking around these subgiants.